Output-only modal dynamic identification of frames by a refined FDD algorithm at seismic input and high damping

Fabio PIOLDI[1], Rosalba FERRARI[1], Egidio RIZZI[1,*]

Submitted: 18 November 2013; Revised: 7 July 2014, 30 January 2015, 15 May 2015

Abstract

The present paper deals with the seismic modal dynamic identification of frame structures by a refined Frequency Domain Decomposition (rFDD) algorithm, autonomously formulated and implemented within *MATLAB*. First, the output-only identification technique is outlined analytically and then employed to characterize all modal properties. Synthetic response signals generated prior to the dynamic identification are adopted as input channels, in view of assessing a necessary condition for the procedure's efficiency. Initially, the algorithm is verified on canonical input from random excitation. Then, modal identification has been attempted successfully at given seismic input, taken as base excitation, including both strong motion data and single and multiple input ground motions. Rather than different attempts investigating the role of seismic response signals in the Time Domain, this paper considers the identification analysis in the Frequency Domain. Results turn-out very much consistent with the target values, with quite limited errors in the modal estimates, including for the damping ratios, ranging from values in the order of 1% to 10%. Either seismic excitation and high values of damping, resulting critical also in case of well-spaced modes, shall not fulfil traditional FFD assumptions: this shows the consistency of the developed algorithm. Through original strategies and arrangements, the paper shows that a comprehensive rFDD modal dynamic identification of frames at seismic input is feasible, also at concomitant high damping.

Keywords: *Modal dynamic identification; Operational Modal Analysis (OMA); Frequency Domain Decomposition (FDD); seismic input; estimated (high) modal damping ratio; frame structures.*

** Corresponding Author, email: egidio.rizzi@unibg.it, fax: +39.035.205.2310, tel. +39.035.205.2325.*

[1] Università degli Studi di Bergamo, Dipartimento di Ingegneria e Scienze Applicate (Dalmine), viale G. Marconi 5, I-24044 Dalmine (BG), Italy.

PART I: Theoretical formulation and computational implementation

1. Introduction

The dynamic characterization of mechanical systems and engineering structures keeps becoming increasingly important towards reaching several focused goals, such as dynamic response prediction, finite element model updating, structural health monitoring, passive and active vibration control, and so on [1], [2], [3], [4], [5].

Dynamic testing allows for a reliable evaluation of basic structural properties, e.g. natural frequencies, mode shapes and damping ratios. In this context, prompt and accurate estimates may be derived from output-only modal identification procedures [6], which belong to a specific branch of modal dynamic identification [7]. This group of procedures pertaining to Operational Modal Analysis (OMA) recurs only to structural response signals induced by undetermined ambient loads (operating loads, wind, turbulence, traffic), in order to determine the corresponding Power Spectral Density (PSD) functions, from which structural modal properties may be extracted [6]. These output-only techniques display two major advantages with respect to more traditional input-output identification techniques in the field of Experimental Modal Analysis (EMA) [8], [1], [9], [10]: no excitation devices are required; all (or part) of the measurements (coordinates) may be used as reference (i.e. as input for the identification algorithm). Thus, OMA identification algorithms belong to Multi-Input-Multi-Output (MIMO) procedures [11]. This allows to detect even closely-spaced or repeated modes, looking for a suitable characterization of real complex structures [12], [13].

The present paper deals with the modal dynamic identification of frame structures by an output-only technique in the frequency domain, i.e. a refined Frequency Domain Decomposition (rFDD) algorithm, implemented autonomously within *MATLAB* [14], [15], starting from the classical description in the original works by Brincker et al. [16], [17], [18]. FDD techniques allow for estimating natural frequencies and mode shapes of the structural system; in their EFDD (Enhanced FDD) formulations [18], [19], [20], also of modal damping ratios and undamped natural frequencies. Recently, a third generation of FDD, i.e. Frequency Spatial Domain Decomposition (FSDD), has been developed to eliminate some disadvantages of EFDD algorithms [13], [21], [22]. However, the algorithm presented in this work refines and rejuvenates classical EFDD algorithms, through specific computational strategies, allowing the structural identification at seismic input and concomitant heavy damping. In this application field, its robustness as compared to traditional EFDD algorithms has been effectively proven.

According to the existing literature, FDD techniques appear to remove typical disadvantages associated to classical frequency domain approaches [6], e.g. they allow to detect close vibration modes and do not result excessively sensitive to ambient noise [19]. The method should work properly within crucial typical hypotheses such as: canonical force input based on stationary Gaussian white noise (i.e. free vibration data or weak stationary ambient excitations), very lightly-damped structures (damping ratios less than 1%) and geometrically orthogonal mode shapes of close modes. Within such assumptions, identified modal properties have been typically related to small-amplitude vibrations [23], [24]. Even so, it is known that dynamic properties of civil structures may result amplitude-dependent; hence, parameters identified from small-amplitude responses may not match those from earthquakes, or generally from strong excitations [25], [26], [23]. These features are pertinent to consistent seismic characterization of civil engineering structures. Then, classical FDD formulations shall not be employed, as they are, for non-stationary response signals such as seismic excitations and for heavy-damped structures [6].

Within the EMA framework, the modal dynamic identification of civil structures under seismic excitation has been pursued in [27], [25], [26], [24]. In the field of OMA, as opposed to different attempts that already investigated the role of seismic response (output) signals in the Time Domain [28], [29], [30], [23], the present research innovatively considers the analysis in the Frequency Domain, through a refined FDD algorithm, with strong motion data recordings used as structural input. Also, high values of damping ratios are concomitantly considered. Such research scenario looks quite challenging in the present dedicated literature, since FDD seems to be lacking on that [31].

In this paper, synthetic response signals generated prior to the dynamic identification (by direct time integration from given input signals) are adopted as input channels for the developed FDD algorithm, in view of assessing a necessary condition for the procedure's efficiency. Then, the algorithm has been attempted at seismic input, taken as base excitation, including for strong motion records and for both single and multiple input ground motions. Though this type of signals and heavy damping should not fit among canonical assumptions of FDD identification, the use of the rFDD algorithm leads to very accurate estimates.

Innovative and key issues of the procedure are originally treated and discussed, e.g. the processing of PSD matrix, the use of untrended correlation functions, the accounting of data filtering. Additionally, frequency resolution effect, spectral bell width, singular value and peak selection, and adopted regression time window of the antitransformed signal have been included. In short, this paper shows that FDD dynamic identification of structural properties at seismic input is feasible, with quite limited errors in the estimates of the modal characteristics, including for (high) modal damping ratios.

By attempting to clear the analytical theory of FDD techniques, following Section 2 outlines first basic steps of the theoretical formulation. Some innovative strategies and features of the refined FDD algorithm are described, too. Section 3 presents the dedicated iterative loop for the modal damping ratio estimates developed within the rFDD algorithm. Preliminary assessment results have been produced in Section 4 for classical white noise input, even at heavy damping. At first, Section 5 shows the characteristics of the strong ground motions taken as base excitation for the frame structures. Interpretations on the use of seismic response signals and heavy damping with the present rFDD algorithm are emphasized. Then, comprehensive results on modal identification at seismic input, including for quite high values of damping, are outlined. Comparison results among the proposed refined FDD algorithm and a classical FDD implementation are presented both in Sections 4 and 5. Further, detailed analyses concerning a realistic structure taken from the literature are produced and reported in Section 6, by considering multiple input earthquake recordings, ground motion data collected at different locations and noise addition to the time signals. Main conclusions are finally gathered in Section 7.

2. Refined FDD technique

The common feature of frequency domain methods is the evaluation of the spectral density functions from the structural system responses. The main difference, on the contrary, is the procedure through modal parameters are extracted from the Power Spectral Density (PSD) matrix. The FDD technique [18], [16] is an extension of the classical frequency domain approach, denominated BFD (Basic Frequency Domain) or also PP (Peak Picking) [6], [17].

The classical frequency approach is based on a DFT (Discrete Fourier Transform) signal processing. The FDD technique is able to pick up close modes with better accuracy and does not result excessively sensitive to ambient noise. It operates a Singular Value Decomposition (SVD) of the PSD matrix on each line of the frequency spectrum, which has the powerful property of separating noisy data from disturbances of various source. The PSD matrix is then decomposed into a set of auto-spectral density functions, each corresponding to a SDOF system, from which natural frequencies and mode shapes can be extracted [32]. Typical characteristic assumptions for the validity of the method are white noise input, very low structural damping ratios (below 1%) and geometrically-orthogonal mode shapes of closed modes. If these assumptions are not satisfied, the SVD decomposition may result approximated, leading to noisy plots and inaccurate results. Previous assumptions and procedures belong to classical FDD implementations, as stated from main literature works as [16], [18], [17], [19], [31], [13], [21]. Even so, the present rFDD algorithm, through its computational procedures, deals also with seismic input and heavy damping conditions. Thus, consistent modal identification becomes truly possible also with signals different from those fulfilling traditional FDD assumptions.

Theoretical developments and implemented original strategies of the rFDD algorithm help to work under those conditions, leading to effective modal parameter estimates. In the current section and in Sections 3 and 5, the underlying theory and computational procedures are explicitly presented and emphasized, jointly with remarks and explanations about the present successful use for earthquake excitation and heavy damping.

2.1 Theoretical framework of FDD techniques (SHORTENED)

In the dedicated literature, original papers have laid down the main strategy of FDD methods, starting from the early works of Brincker et al. [6], [16], [17], [21]. The present section gathers and re-elaborates the fundamental concepts on the subject, with the purpose of providing a general, clear and unitary theoretical framework of FDD techniques, adopted here as basis for the present refined FDD formulation. This attempt is felt original, since this seems to be lacking in the present literature, where often erroneous statements and formulations are repeated in series by various authors, referring to others, without any direct assessment and inspection. In the present paper, all crucial steps and equations are consistently exposed and derived in a self-contained manner, with respect to continuous time and spatial scale. Whereas it is necessary for a better understanding, steps arising from the numerical implementation, i.e. to discrete time, have been added.

The FDD theory is based on the input/output relationship of a stochastic process for a general n-dof system [33]:

$$\mathbf{G}_{yy}(\omega) = \bar{\mathbf{H}}(\omega)\mathbf{G}_{xx}(\omega)\mathbf{H}^{T}(\omega) \tag{2.1}$$

where $\mathbf{G}_{xx}(\omega)$ and $\mathbf{G}_{yy}(\omega)$ are the $(r \times r)$ and $(m \times m)$ input and output PSD matrices, respectively, r the number of input channels (references) and m the number of output responses (measurements). The overbar denotes complex conjugate, and apex symbol T transpose. Then, $\mathbf{H}(\omega)$ is the $(m \times r)$ Frequency Response Function (FRF) matrix, which may be also written in pole/residue form [1]:

$$\mathbf{H}(\omega) = \sum_{k=1}^{n} \frac{\mathbf{R}_k}{i\omega - \lambda_k} + \frac{\bar{\mathbf{R}}_k}{i\omega - \bar{\lambda}_k} \tag{2.2}$$

where n is the number of modes, $\lambda_k = -\zeta_k\omega_k + i\omega_{dk} = -\zeta_k\omega_k + i\omega_k\left(1-\zeta_k^2\right)^{1/2}$, $\bar{\lambda}_k$ are the poles (in complex conjugate pairs) of the FRF and $\mathbf{R}_k = \boldsymbol{\phi}_k\boldsymbol{\Gamma}_k^{T}$ the $(m \times r)$ residue matrix [1], [16]. In these formulations ζ_k is the modal damping ratio, and ω_k and ω_{dk} are the undamped and damped angular frequencies associated to the k^{th} pole. Then, $\boldsymbol{\phi}_k = [\phi_{1k}\ \phi_{2k} \dots \phi_{Nk}]^T$ and $\boldsymbol{\Gamma}_k = [\Gamma_{1k}\ \Gamma_{2k} \dots \Gamma_{Rk}]^T$ are the k^{th} $(m \times 1)$ mode shape vector and $(r \times 1)$ modal participation factor vector, respectively. When all output measurement points are taken as references (i.e. $m = r$), $\dim(\boldsymbol{\phi}_k) = \dim(\boldsymbol{\Gamma}_k)$, so $\mathbf{H}(\omega)$ becomes a square matrix. Then, Eq. (2.1), through Eq. (2.2), can be rewritten as [15]:

$$\mathbf{G}_{yy}(\omega) = \sum_{k=1}^{n}\sum_{s=1}^{n}\left(\frac{\bar{\mathbf{R}}_k G_{xx}}{-i\omega - \bar{\lambda}_k} + \frac{\mathbf{R}_k G_{xx}}{-i\omega - \lambda_k}\right)\left(\frac{\mathbf{R}_s^{T}}{i\omega - \lambda_s} + \frac{\mathbf{R}_s^{H}}{i\omega - \bar{\lambda}_s}\right) \tag{2.3}$$

where Hermitian apex symbol H denotes complex conjugate and transpose. This is feasible since the PSD matrix $\mathbf{G}_{xx}(\omega)$ *is constant in case of stationary zero mean white noise input* [33]; Then, remembering also the PSD computation by the Short Time Fourier Transform [33], $\mathbf{G}_{xx}(\omega)$ becomes real valued and non-negative, so that $\mathbf{G}_{xx}(\omega) \Rightarrow G_{xx} = \bar{G}_{xx}$. Thus, by recalling the properties of $\mathbf{G}_{xx}(\omega)$ and by applying the Heaviside partial fraction expansion theorem to Eq. (2.3), one can obtain the final pole/residue form of the output PSD matrix [12]:

$$\mathbf{G}_{yy}(\omega) = \sum_{k=1}^{n} \frac{\mathbf{A}_k}{i\omega - \lambda_k} + \frac{\mathbf{A}_k^{H}}{-i\omega - \bar{\lambda}_k} + \frac{\bar{\mathbf{A}}_k}{i\omega - \bar{\lambda}_k} + \frac{\mathbf{A}_k^{T}}{-i\omega - \lambda_k} \tag{2.4}$$

where $\mathbf{A}_k$ is the residue matrix of the PSD output corresponding to the k^{th} pole λ_k. As for the PSD output itself, the residue matrix is an $(m \times m)$ Hermitian matrix given by [13]:

$$\mathbf{A}_k = \sum_{s=1}^{n}\left(\frac{\mathbf{R}_s}{-\lambda_k - \lambda_s} + \frac{\bar{\mathbf{R}}_s}{-\lambda_k - \bar{\lambda}_s}\right) G_{xx}\mathbf{R}_k^{T} \tag{2.5}$$

When the structure is lightly damped (small damping ratios $\zeta_k \ll 1$), the pole can be expressed as $\lambda_k = -\zeta_k\omega_k + i\omega_{dk} \cong -\zeta_k\omega_k + i\omega_k$; then, in the vicinity of the k^{th} modal frequency the residue matrix can be expressed by the following approximate expression [13], [15]:

$$\mathbf{A}_k = \left[\frac{\mathbf{R}_k}{2(\zeta_k\omega_k - i\omega_k)} + \frac{\bar{\mathbf{R}}_k}{2\zeta_k\omega_k}\right] G_{xx}\mathbf{R}_k^T \simeq \frac{\bar{\mathbf{R}}_k G_{xx}\mathbf{R}_k^T}{2\zeta_k\omega_k} = \frac{\bar{\boldsymbol{\phi}}_k \boldsymbol{\Gamma}_k^H G_{xx}\boldsymbol{\Gamma}_k \boldsymbol{\phi}_k^T}{2\zeta_k\omega_k} = d_k\bar{\boldsymbol{\phi}}_k\boldsymbol{\phi}_k^T \qquad (2.6)$$

where only the $\bar{\mathbf{R}}_k$ term survives, since the $\zeta_k\omega_k$ denominator is dominant with respect to the $2(\zeta_k\omega_k - i\omega_k)$ one, and the term: $d_k = (\boldsymbol{\Gamma}_k^H G_{xx}\boldsymbol{\Gamma}_k)/(2\zeta_k\omega_k)$ is a real scalar. Then, with the formulation of Eq. (2.6), the residue matrix $\mathbf{A}_k$ becomes proportional to a matrix based on the mode shape vector, i.e. $\mathbf{A}_k \propto \bar{\mathbf{R}}_k G_{xx}\mathbf{R}_k^T = \bar{\boldsymbol{\phi}}_k\boldsymbol{\Gamma}_k^H G_{xx}\boldsymbol{\Gamma}_k\boldsymbol{\phi}_k^T \propto d_k\bar{\boldsymbol{\phi}}_k\boldsymbol{\phi}_k^T$. So, by substituting Eq. (2.6) into (2.4) one derives:

$$\mathbf{G}_{yy}(\omega) = \sum_{k=1}^{n} \frac{d_k\bar{\boldsymbol{\phi}}_k\boldsymbol{\phi}_k^T}{i\omega - \lambda_k} + \frac{d_k\bar{\boldsymbol{\phi}}_k\boldsymbol{\phi}_k^T}{-i\omega - \bar{\lambda}_k} + \frac{d_k\boldsymbol{\phi}_k\boldsymbol{\phi}_k^H}{i\omega - \bar{\lambda}_k} + \frac{d_k\boldsymbol{\phi}_k\boldsymbol{\phi}_k^H}{-i\omega - \lambda_k} \qquad (2.7)$$

In the narrow band with spectrum lines in the vicinity of a modal frequency, only the first two terms in Eq. (2.8) are dominant, since their denominators $-i\omega - \bar{\lambda}_k = \overline{i\omega - \lambda_k} \simeq \zeta_k\omega_k$ are smaller with respect to the last two, $i\omega - \bar{\lambda}_k = \overline{-i\omega - \lambda_k} \simeq \zeta_k\omega_k + 2i\omega_k$. Taking this into account, the previous equation can be simplified as:

$$\mathbf{G}_{yy}(\omega) \simeq \sum_{k=1}^{n} \frac{d_k\bar{\boldsymbol{\phi}}_k\boldsymbol{\phi}_k^T}{i\omega - \lambda_k} + \frac{d_k\bar{\boldsymbol{\phi}}_k\boldsymbol{\phi}_k^T}{-i\omega - \bar{\lambda}_k} = \bar{\boldsymbol{\Phi}}\left\{\mathrm{diag}\left[\Re e\left(\frac{2d_k}{i\omega - \lambda_k}\right)\right]\right\}\boldsymbol{\Phi}^T \qquad (2.8)$$

where $\boldsymbol{\Phi} = [\boldsymbol{\phi}_1\ \boldsymbol{\phi}_2\ \ldots \boldsymbol{\phi}_n]$ is the eigenvector matrix, gathering all the eigenvectors $\boldsymbol{\phi}_i$ as columns. Eq. (2.8) represents a modal decomposition of the spectral matrix. The contribution to the spectral density matrix from a single mode k can be expressed as:

$$\mathbf{G}_{yy}(\omega_k) \simeq \bar{\boldsymbol{\phi}}_k\left\{\mathrm{diag}\left[\Re e\left(\frac{2d_k}{i\omega - \lambda_k}\right)\right]\right\}\boldsymbol{\phi}_k^T = \bar{\boldsymbol{\phi}}_k\left\{\mathrm{diag}\left[\frac{2d_k\zeta_k\omega_k}{(\zeta_k\omega_k)^2 + (\omega - \omega_{dk})^2}\right]\right\}\boldsymbol{\phi}_k^T \qquad (2.9)$$

This final form is then decomposed, using the SVD technique, into a set of singular values and their corresponding singular vectors. From the former, natural frequencies are extracted; from the latter, approximate mode shapes are obtained. The present unitary treatment, though largely based on existing FDD literature, has attempted to highlight all key steps in the formulation, achieving the derivation of all needed equations and operators.

2.2 Modal identification through a refined FDD algorithm (SHORTENED)

The time domain counterpart of the PSD in Eq. (2.4) is the correlation function matrix $\mathbf{R}_{yy}(\tau)$, starting point of the developed FDD algorithm [13]:

$$\mathbf{R}_{yy}(\tau) = \mathcal{F}^{-1}\{\mathbf{G}_{yy}(\omega)\} = \sum_{k=1}^{n} \mathbf{A}_k e^{\lambda_k\tau} + \bar{\mathbf{A}}_k e^{\bar{\lambda}_k\tau} - \mathbf{A}_k^T e^{-\lambda_k|\tau|} - \mathbf{A}_k^H e^{-\bar{\lambda}_k|\tau|} \qquad (2.10)$$

It is possible to generate the FDD representation also from time domain entries (i.e. accelerations, as considered here), by expressing the structural response $\mathbf{y}(t)$ in terms of modal coordinates:

$$\mathbf{y}(t) = \sum_{k=1}^{n} \boldsymbol{\phi}_k p_k(t) = \boldsymbol{\Phi}\mathbf{p}(t) \qquad (2.11)$$

where $\mathbf{p}(t)$ is the vector of principal coordinates $p_k(t)$. The response signals are correlated in order to obtain the matrix of auto- and cross-correlation functions, $\mathbf{R}_{yy}(\tau)$:

$$\mathbf{R}_{yy}(\tau) = E[\bar{\mathbf{y}}(t+\tau)\mathbf{y}(t)^T] = E[\bar{\boldsymbol{\Phi}}\bar{\mathbf{p}}(t+\tau)\mathbf{p}(t)^T\boldsymbol{\Phi}^T] = \bar{\boldsymbol{\Phi}}\mathbf{R}_{pp}(\tau)\boldsymbol{\Phi}^T \qquad (2.12)$$

where $\mathbf{R}_{pp}(\tau) = E[\bar{\mathbf{p}}(t+\tau)\mathbf{p}(t)^T]$ is the auto- and cross-correlation response matrix, in principal coordinates. The $\mathbf{R}_{yy}(\tau)$ matrix in Eq. (2.12) can be calculated numerically, for a finite signal length, with the following estimator [33]:

$$\mathbf{R}_{\mathrm{yy}}(\tau) \simeq \frac{1}{t}\sum_{t=1}^{t-\tau} \bar{\mathbf{y}}(t+\tau)\mathbf{y}(t)^{\mathrm{T}} \tag{2.13}$$

where instant τ spans from 0 to t, i.e. $0 \leq \tau < t$. In presence of noisy or weakly-stationary data (or non-stationary data, as the earthquake response signals treated here), the $\mathbf{R}_{\mathrm{yy}}(\tau)$ matrix can be further processed to obtain an untrended (and unbiased) well-defined version. This expedient helps in removing possible troubles related to weakly-stationary or non-stationary data and leads to a refinement of the subsequent estimates [34].

The formulations in Eq. (2.12) are transformed into the frequency domain by Fourier Transform, to obtain the PSD matrix of responses, $\mathbf{G}_{\mathrm{yy}}(\omega)$, through the so-called Wiener-Khinchin theorem [33]:

$$\mathbf{G}_{\mathrm{yy}}(\omega) = \mathcal{F}\left[\mathbf{R}_{\mathrm{yy}}(\tau)\right] = \mathcal{F}\left[\bar{\boldsymbol{\Phi}}\mathbf{R}_{\mathrm{pp}}(\tau)\boldsymbol{\Phi}^{\mathrm{T}}\right] = \bar{\boldsymbol{\Phi}}\mathbf{G}_{\mathrm{pp}}(\omega)\boldsymbol{\Phi}^{\mathrm{T}} \tag{2.14}$$

where $\mathbf{G}_{\mathrm{pp}}(\omega)$ is the PSD matrix of the input (in principal coordinates). The PSD matrix of responses in Eq. (2.14) can be calculated numerically, for a finite signal length, by the Fast Fourier Transform (FFT) algorithm, via a Cooley-Tukey procedure. Rather than steps from Eq. (2.11) to Eq. (2.14), which may be named as Wiener-Khinchin approach, another common way to obtain an estimate of the PSD matrix of responses, $\mathbf{G}_{\mathrm{yy}}(\omega)$, is the so-called Welch Modified Periodogram method [35].

Differently from the Wiener-Khinchin procedure, the Welch approach implements signal sectioning, windowing and overlapping before the frequency domain convolution [35]. The present refined FDD algorithm displays the powerful feature of implementing both PSD computations. The Wiener-Khinchin algorithm generally returns well-defined peaks, providing the best results with very short signals, as for earthquake records. The Welch approach, instead, thanks to averaging and to the use of smoothing windows, leads to slightly better estimates, especially towards treating long recordings, but sometimes may lead to noisier SVs [34]. According to the characteristics of the acquired structural responses, the joint use of these two techniques effectively helps in the estimates, by combining their advantages, especially at seismic input and heavy damping.

Now, as it is common in stochastic dynamics [13], it is possible to assume that the modal coordinates are un-correlated; leading to $\mathbf{R}_{\mathrm{pp}}(\tau)$ and $\mathbf{G}_{\mathrm{pp}}(\omega)$ diagonal matrices. Then, if the mode shapes (the columns of matrix $\boldsymbol{\Phi}$) are orthogonal, Eq. (2.14) represents a spectral decomposition, achieving for the SVD of the transpose of the PSD matrix:

$$\mathbf{G}_{\mathrm{yy}}^{\mathrm{T}}(\omega) \simeq \boldsymbol{\Phi}\left\{\mathrm{diag}\left[\Re\mathrm{e}\left(\frac{2\mathrm{d}_{\mathrm{k}}}{\mathrm{i}\omega - \lambda_{\mathrm{k}}}\right)\right]\right\}\boldsymbol{\Phi}^{\mathrm{H}} = \mathbf{USU}^{\mathrm{H}} \tag{2.15}$$

where $\mathbf{U}$ is a unitary complex matrix (i.e. $\mathbf{UU}^{\mathrm{H}} = \mathbf{U}^{\mathrm{H}}\mathbf{U} = \mathbf{I}$) holding the singular vectors (i.e. the eigenvectors) and $\mathbf{S}$ is a real diagonal matrix holding the singular values (i.e. the eigenvalues), defining a factorization which is known as spectral theorem [1], [13]. The above mentioned SVD technique is performed at each single frequency line, i.e. at discrete frequencies $\omega = \omega_{\mathrm{i}}$.

Starting from the SVD of Eq. (2.15), modal identification can be made around a modal peak in the frequency domain, which can be located by a peak-picking procedure on the SV plot, as it is shown in Fig. 1a. The peak-picking can also be performed on the SV product plot, as originally treated in [15], according to a procedure that supports the identification in case of heavy damping or noisy data and improves the results. Then, when only the k^{th} principal value is dominant, i.e. it reaches the maximum near the modal frequency ω_{k}, the PSD can be approximated by a unitary rank matrix [6], [16]:

$$\mathbf{G}_{\mathrm{yy}}^{\mathrm{T}}(\omega_{\mathrm{i}} = \omega_{\mathrm{k}}) \simeq \mathrm{s}_{\mathrm{k}}\mathbf{u}_{\mathrm{k1}}\mathbf{u}_{\mathrm{k1}}^{\mathrm{H}} \tag{2.16}$$

where the first singular value at the k^{th} resonance frequency provides an estimate, with unitary normalization, of the related mode shape, i.e. $\widehat{\boldsymbol{\phi}}_{\mathrm{k}} = \mathbf{u}_{\mathrm{k1}}$. The identified mode shape is then compared to the others in its proximity [36], in terms of MAC (Modal Assurance Criterion) index [37], which represents the square of the correlation between two modal vectors $\boldsymbol{\phi}_{\mathrm{r}}$, $\boldsymbol{\phi}_{\mathrm{s}}$ This allows to nearby investigate the dominant mode: in fact, if the mode is effectively dominant, the mode shape for that interval does not vary, locating a subset of SV that belongs to the SDOF density function [13].

3. Refined FDD algorithm in MATLAB environment

Pseudo-experimental synthetic response signals generated prior to the dynamic identification are adopted as numerical input for the FDD algorithm. Random noise or seismic excitation are assumed as loading at the base of the structures, which are taken as multi-storey shear type frames (Appendix A). This is done in view of assessing a first necessary condition for the procedure's efficiency. The structural response of the frame systems is solved by direct integration with Newmark's (average acceleration) method. Then, the adopted modal identification procedure implemented within *MATLAB* consists of two fundamental phases:

1. The simulated responses (storey accelerations) are used as input channels for the rFDD algorithm: the estimates of natural damped frequencies and mode shapes are evaluated (first part of the rFDD algorithm, see Section 2.2).
2. The rFDD algorithm is further extended, achieving modal damping ratios and undamped natural frequencies estimates through an iterative optimization procedure. This part is treated next.

3.1 Classical Enhanced FDD algorithm

With the EFDD algorithm [18], [17], further development of the FDD technique, modal damping ratios and undamped frequencies can be evaluated. The singular value of the estimated mode shape represents the PSD function of the corresponding SDOF system [16]. Thus, a classical EFDD algorithm is implemented according to the main phases below. Instead, the present rFDD develops an iterative loop of advanced optimization to improve modal damping ratio estimates. This is presented later in Section 3.2.

The PSD function is identified around the resonance peak, comparing the associated mode shape estimate with those at nearby frequency lines, in terms of MAC filtering [17], [19]. This phase is usually referred to as spectral bell identification. A sample of the procedure is shown in Fig. 1b.

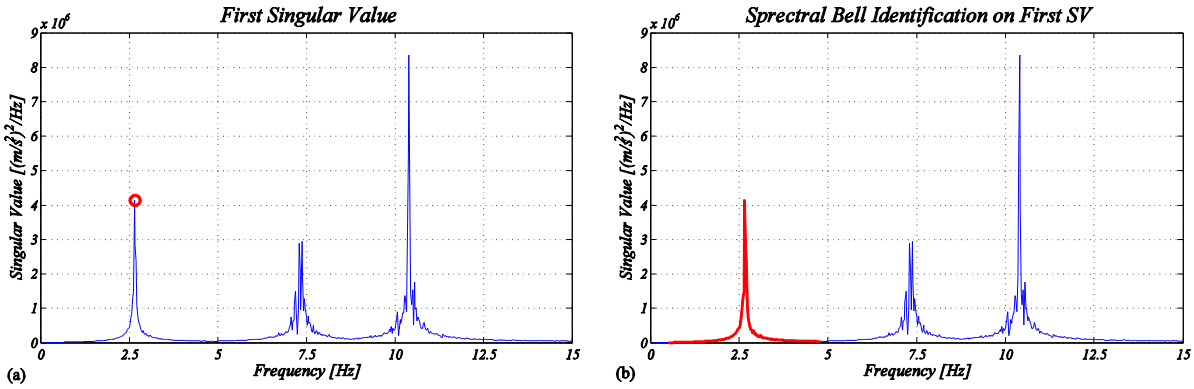

Figures 1a, 1b: *Peak-picking and spectral bell identification of the first mode shape; first singular value, three-storey frame, random input.*

The located subset of singular values in the spectral bell is taken back to the time domain by Inverse Discrete Fourier Transform (IDFT), by obtaining an estimate of the Auto-Correlation Function (ACF) of the antitransformed signal, i.e. the ACF of the SDOF system related to the resonance peak. In this process, the remaining parts of the PSD function laying outside the spectral bell frequency window are set to zero [18].

The antitransformed signal is normalized, dividing by its maximum value. All extrema, i.e. peaks and valleys, representing the free decay of a damped SDOF system, are identified within an appropriate time window, as it can be seen in a sample in Fig. 2a. The first two peaks and valleys must be excluded. Indeed, they may induce errors in subsequent operations [6], [21], [14]. Through peak- and valley-picking in the selected time window, it is possible to assess the logarithmic decrement δ:

$$\delta = \frac{2}{k} \ln\left(\frac{r_0}{|r_k|}\right) \tag{3.1}$$

where k is an integer index counter of the k^{th} extreme of the auto-correlation function, k = 1,2,3, ..., while r_0 and r_k are the initial and the k^{th} extreme value of the auto-correlation function, respectively. Then, it is possible to obtain a linear relation in terms of index k [20], [14]:

$$2\ln(|r_k|) = 2\ln(r_0) - \delta\, k \tag{3.2}$$

which can be plotted and fitted with a straight line (see a sample in Fig. 2b). The logarithmic decrement δ is then estimated as the slope of this straight line through linear regression on k and $2\ln(|r_k|)$. Finally, from the estimated logarithmic decrement δ_q of the q^{th} mode the corresponding modal damping ratio can be classically evaluated as:

$$\zeta_q = \frac{\delta_q}{\sqrt{4\pi^2 + \delta_q^2}} \tag{3.3}$$

Knowing the estimated damping ratio and the estimated damped frequencies, also the undamped natural frequency can be obtained [18]. Summarizing, the standard EFDD algorithm sets fixed values for the MAC index (for example 0.6) used to perform the spectral bell ID and the peaks of the auto-correlation within 90% to 20% of the maximum amplitude were selected to perform subsequent regression operations. More details on the standard procedure may be found in [18], [38], [20].

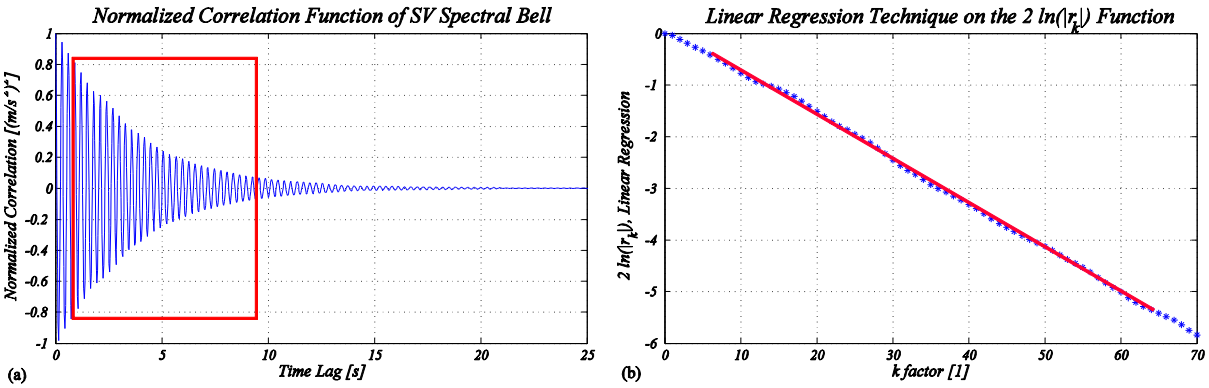

Figures 2a, 2b: *Representation of the selected time window over the normalized IDFT and of the linear regression over* k *and* $2\ln(r_k)$*; first singular value, three-storey frame, random input.*

3.2 Iterative loop and optimization algorithm for the modal damping ratio estimates

The following procedure is fundamental in order to achieve reliable computational estimates of the modal damping ratios in case of earthquake response input and heavy damping, which adversely affects the correct working of traditional EFDD algorithms. Especially, the use of preselected fixed parameters [34] (i.e. MAC value for the bell ID and selected range of amplitudes for the auto-correlation function, as explained in the previous section) as usually done in standard EFDD techniques is not adequate for such challenging conditions [38], [20]. Also, the use of seismic input makes it harder for the correct detection of the SDOF system associated to the identified mode. Besides, the use of the following procedure automates the estimation of the modal damping ratios and does not require the interaction with an expert operator.

The selection of the correct time window on the SDOF Auto-Correlation Function (ACF) represents the most difficult part of the algorithm. Jointly with the spectral bell identification, these operations derive from truncated data and might introduce bias errors in the damping estimates. This disadvantage must be taken into account especially with closely spaced modes [21]. An inspection about contents, decimation and frequency resolution must be necessary to achieve clear time window representations [14], as treated in Section 5.

Besides, the correct outcome of the linear regression operation in Eq. (3.2) is directly connected to the adequacy of the time window selection. These two steps, jointly with the choice of the spectral bell, shall be performed by an *iterative operation of advanced optimization*, as outlined below:

1. The identification of the spectral bell related to the q^{th} mode of vibration is set first with a 0.9 MAC confidence level, by defining the related subset of SVs, $\mathbf{S}_Q$, directly from Eq. (2.14):

$$\mathrm{MAC}(\boldsymbol{\phi}_r, \boldsymbol{\phi}_q) \geq 0.90 \;\Rightarrow\; \mathbf{S}_Q(\omega) = \mathbf{S}(\omega_i = \omega_q)_{[m\times 1]} = \left[\mathbf{0}\ s_l\ \cdots\ s_q\ \cdots\ s_u\ \mathbf{0}\right]^T \tag{3.4}$$

where s_l and s_u are the lower and upper values of the spectral bell.

2. According to the standard EFDD formulation, the identified set of the SV is antitransformed back to the time domain and then normalized, by obtaining the related SDOF ACF, $\mathbf{R}_{yy,Q}(\tau)$:

$$\mathbf{R}_{yy,Q}(\tau) = \mathcal{F}^{-1}\{\mathbf{S}_Q(\omega)\} = \frac{1}{m}\sum_{j=0}^{m-1} \mathbf{S}_Q(\omega) e^{-\frac{2\pi i}{m}jl} = [r_1\ \cdots\ r_m]^T, \quad l = 1, \dots, m-1 \tag{3.5}$$

3. On the graph of the obtained normalized SDOF ACF, two exponential decays are fitted (by the use of *MATLAB* command *fit*), both on peaks and valleys of the ACF. The exponential fitting model is calculated for both peaks and valleys, $\hat{\mathbf{y}}_p$ and $\hat{\mathbf{y}}_v$, respectively:

$$\hat{\mathbf{y}}_p = A_p \exp(B_p \mathbf{x}_p), \quad \hat{\mathbf{y}}_v = A_v \exp(B_v \mathbf{x}_v) \tag{3.6}$$

where $\mathbf{x}_i$ represent the vector of peak and valley time instants and A_i and B_i are the parameters to be fitted. They can be calculated by the minimization of the R function as follows:

$$R^2(a,b) = \sum_{j=1}^{m} y_j\left[\ln(y_j) - (a + b x_j)\right]^2 \;\Rightarrow\; J = \frac{\partial(R^2)}{\partial a_i} = 0 \tag{3.7}$$

with coefficients $a = \ln(A)$ and $b = B$. Solving for a and b, it is possible to obtain the estimates of the exponential decays, $\hat{\mathbf{y}}_p$ and $\hat{\mathbf{y}}_v$, as in Eq. (3.6).

4. All extrema, i.e. peaks and valleys of the ACF, ranging from r_0 = 90% to r_n = 30% of the maximum amplitude are selected within a time window, by achieving the subset $\mathbf{R}_{yy,Q}(\tau_{sub})$ from the normalized ACF:

$$r_n = 0.3 \leq \mathbf{R}_{yy,Q}(\tau) \leq r_0 = 0.9 \;\Rightarrow\; \mathbf{R}_{yy,Q}(\tau_{sub}) = [r_0\ \cdots\ r_n]^T \subseteq \mathbf{R}_{yy,Q}(\tau) \tag{3.8}$$

5. Subsequent operations of regression, according to Eq. (3.2), are performed and the modal damping ratio ζ_q is estimated.

6. The exponential decays of Eq. (3.6) included in the time window of the ACF are compared with the classical damping trends:

$$\begin{aligned} \mathbf{y}_p &= \exp(-\zeta_q \omega_q \mathbf{x}_p) = \exp\left[-\zeta_q \frac{\omega_{dq}}{(1-\zeta_q^2)^{1/2}} \mathbf{x}_p\right] \\ \mathbf{y}_v &= -\exp(-\zeta_q \omega_q \mathbf{x}_v) = -\exp\left[-\zeta_q \frac{\omega_{dq}}{(1-\zeta_q^2)^{1/2}} \mathbf{x}_v\right] \end{aligned} \tag{3.9}$$

where the maximum amplitude of the motion is set equal to 1 for the normalized ACF, ζ_q is the estimated modal damping ratio (Step 5) and ω_{dq} is the estimated damped frequency.

7. Eqs. (3.9) derive from the exponential decay of the free damped vibrations of a SDOF system, and are used to compare these calculated decays with the fitted decays of Step 3, by computing the residuals $\boldsymbol{\varepsilon}_i$ between them:

$$\boldsymbol{\varepsilon}_p = \mathbf{y}_p - \hat{\mathbf{y}}_p, \quad \boldsymbol{\varepsilon}_v = \mathbf{y}_v - \hat{\mathbf{y}}_v \tag{3.10}$$

8. The optimization algorithm works in order to minimize these residuals, by recalibrating the time window parameters (i.e. the ACF amplitudes r_0 and r_n) and the MAC confidence level with an iterative loop from Step 1 to Step 7, until a reliable estimate of δ_q, i.e. of ζ_q, is obtained. Then, the residuals must be less than a fixed parameter $\bar{\varepsilon}$, for example $\boldsymbol{\varepsilon}_i < \bar{\boldsymbol{\varepsilon}} = 0.01$:

$$\boldsymbol{\varepsilon}_p = f(\mathrm{MAC}, r_0, r_n) \leq \bar{\boldsymbol{\varepsilon}}, \quad \boldsymbol{\varepsilon}_v = f(\mathrm{MAC}, r_0, r_n) \leq \bar{\boldsymbol{\varepsilon}} \tag{3.11}$$

The MAC index is the first value that is recalibrated by the algorithm, ranging from 0.70 to 0.99, while secondarily r_0 and r_n shall assume values between $0.7 \leq r_0 \leq 1.0$ and $0.1 \leq r_n \leq 0.4$, until the residuals have been minimized.

Specifically, the optimization algorithm used for the minimization of the residuals adopts two sources of information, i.e. the classical damping trends $\mathbf{y}_p$, $\mathbf{y}_v$ and the exponential fitted decays $\hat{\mathbf{y}}_p$, $\hat{\mathbf{y}}_v$. These data depend on the MAC index and ACF time window parameters selected for the analyses. Then, the minimization of the residuals is measured through the following objective function $P(\mathbf{z})$:

$$P(\mathbf{z}) = \left[\alpha \left(\frac{\boldsymbol{\varepsilon}_{p,i}}{\mathbf{y}_{p,i}} \right)^2 , (1-\alpha) \left(\frac{\boldsymbol{\varepsilon}_{v,i}}{\mathbf{y}_{v,i}} \right)^2 \right]^T , \quad i = 1, \dots, n \tag{3.12}$$

where $\mathbf{z}$ is the (3×1) vector including the parameters to be optimized, n being the number of ACF points, and $\alpha \in [0,1]$ is a weigh coefficient, which has been set equal to 0.5 for the result derived in the present work. The residual minimization in the objective function is performed by using the *lsqnonlin* command within *MATLAB*, which implements non-linear least-squares.

This iterative procedure conceptually derives from classical EFDD algorithms [16], [18], but considers a computationally efficient procedure with integrated double loop, which is implemented originally here in the present refined FDD algorithm. This procedure reduces errors in the achieved estimates, with respect to classical EFDD procedures in the literature [18], [38], leading to accurate evaluations of the modal damping ratios, especially for the challenging case of seismic input and heavy damping. Examples of these fitting procedures over the ACF at heavy damping are reported in Figs. 4b and 18b, with random and seismic input, respectively. A flow chart of the proposed rFDD algorithm is finally sketched in Fig. 3.

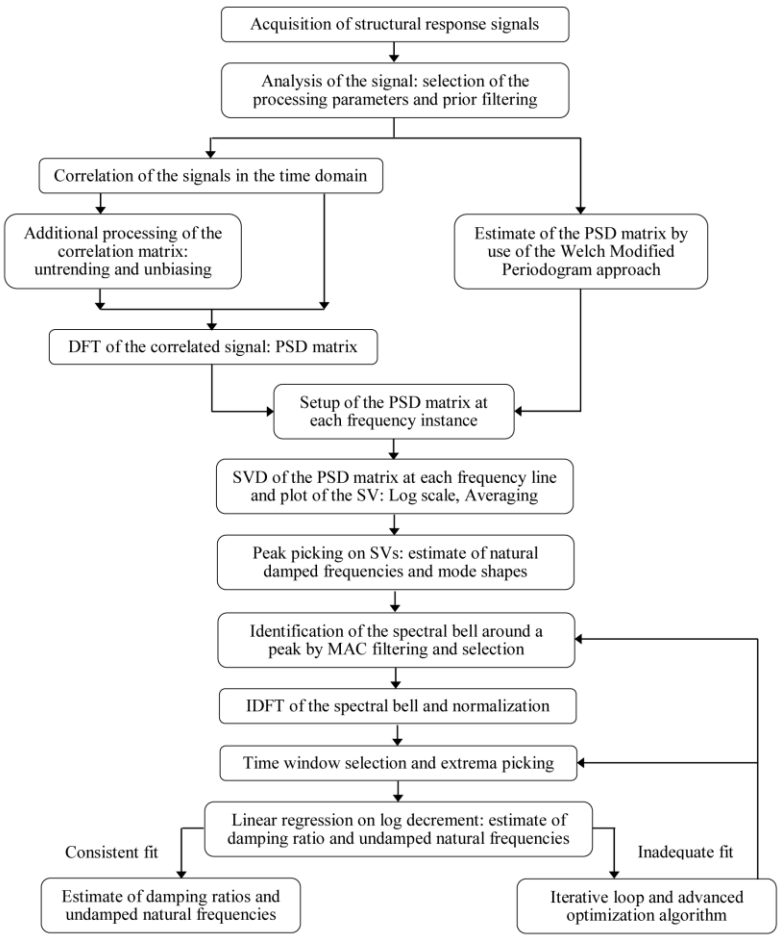

Figure 3: *Flow chart of the proposed refined FDD algorithm.*

4. Validation with random excitation

A series of multi-storey shear-type frames with different structural features has been analyzed first [39], [14], [15]. Results are reported for two-, three- and six-storey frames (Appendix A), which present well-separated modes. The realistic structural model analyzed later in Section 6 is instead characterized by very close modes, and it has been successfully analyzed at random input, too. Using these models, trials with canonical white noise and seismic input have been performed as well to verify the robustness of the developed algorithm. The dynamic parameters are determined before identification via direct modal analysis, taking damping ratios from 1% to 5% and up (until 10% in some cases). Notice that high values of damping are critical not only for closely-spaced modes, but also for well-separated modes, due to the peak flattening and the appearance of extremely noisy SVs. In the FDD literature, whatever the examined structural features, only modal damping ratios below 2% are generally treated [18], [16], [17], [19], [38], [20]. A theoretical demonstration of the rFDD application at heavy damping is suggested in Section 5.1, emphasizing the value of the present approach in such a challenging framework.

Input is taken as a stationary random force at the base, characterized by a uniform frequency spectra. This excites all the structural modes, which can be identified all, through their resonance peaks, into the first singular value of the SVD. The modal information is also included in subsequent SVs, but these are not generally employed to prevent noise occurrence in the results. This phase is required in view of assessing a first necessary condition for the efficiency of the developed algorithm. High values of damping have been already adopted at this step. Following Fig. 4 shows the SVD and the ACF curve-fitting procedure of a three-storey frame with ζ_k = 10%. Dealing with heavy damping, for the iterative procedure the MAC confidence level is set first to 0.8, and the extrema of the ACF ranging from 95% to 15% of its maximum amplitude are selected within the regression time window, allowing to speeding up the convergence of the iterative algorithm. At lower damping it is necessary to adopt a fine frequency resolution in the PSD evaluation, to score correctly the very sharp peaks. To reduce the frequency resolution, it is possible to increase the total length of the acquisitions, operation that however increases the number of computations. In the literature, it is generally said that time recordings lasting about 1000-2000 times the first natural period of the structure often results to be appropriate [8]. In [14] some case studies related record lengths to damping ratio estimates. Results for random input turn-out very much consistent. Some examples with high values of damping are shown in Tables 1a, 1b. Comprehensive results on random input can be found in [15], [34].

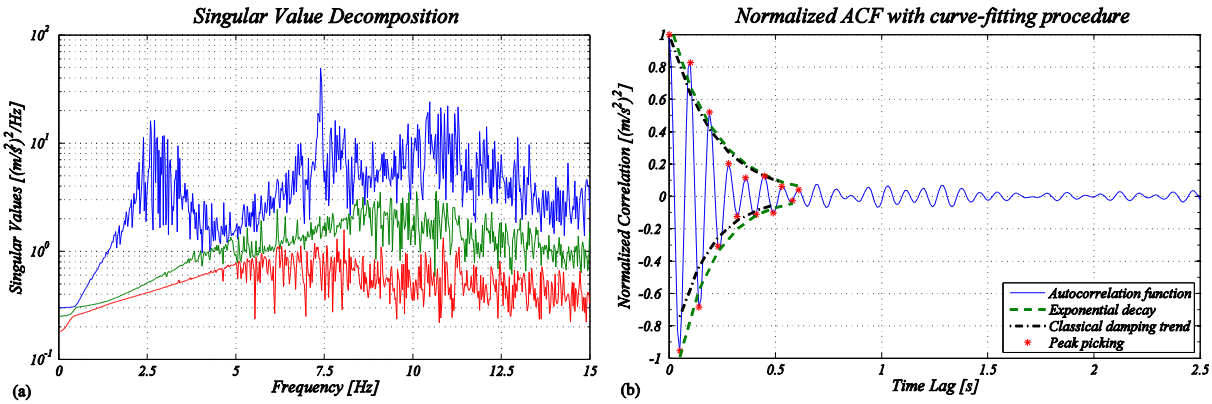

Figures 4a, 4b: *Display of the SVD and of the normalized ACF curve fitting procedure for the third mode of vibration (target damping ratio ζ_k= 10%), three-storey frame, random input.*

The adopted parameters in the processing are the following:

- *Two-storey frame:* Length of time series $t = 400$ s, Sampling frequency $f_s = 200$ Hz, Adopted Frequency resolution $\Delta f = 0.0025$ Hz;
- *Three-storey frame:* Length of time series $t = 600$ s, Sampling frequency $f_s = 200$ Hz, Adopted Frequency resolution $\Delta f = 0.00167$ Hz;

- *Six-storey frame:* Length of time series $\mathrm{t} = 1000\,\mathrm{s}$, Sampling frequency $f_s = 200\,\mathrm{Hz}$, Adopted Frequency resolution $\Delta f = 0.001\,\mathrm{Hz}$.

The efficiency of the developed algorithm is verified, with effective estimates of all the structural modal parameters. The mode shape estimates are remarkable, with MAC indexes always greater than 0.95. The use of the SV product plot may further improve the estimates, especially for the mode shapes [15]. The deviations of the natural frequency estimates are always less than 5%. Similarly, for the damping ratios the average deviation is less than 10%. At variable damping, estimates are obviously better at lower damping, but also appropriate for higher damping. The estimates arising from the developed algorithm are appreciably better, as compared to traditional EFDD algorithms, formulated according to the classical literature [18], [19], [17]. However, for the latter the MAC index is often lower than 0.90 and the deviation of the natural frequency estimates runs sometimes over 5%. Further, especially for the heavy-damped cases, the modal damping ratios estimates display deviations up to 30% for the first modes, while often fail for the higher modes. Thus, for the examined cases, the developed algorithm returns noticeable results without any data filtering before the identification procedure.

Two-storey frame – Random input (ζ_k = 10%)					Δ% - MAC
I mode	Target frequency	4.210 Hz	Estimated frequency	4.114 Hz	2.28%
II mode	Target frequency	10.92 Hz	Estimated frequency	10.58 Hz	3.11%
I mode	Target mode shape	0.5176 0.8557	Estimated mode shape	0.5317 0.8469	1.000
II mode	Target mode shape	-0.8557 0.5176	Estimated mode shape	-0.8597 0.5107	1.000
I mode	Target damping ratio	10.00%	Estimated damping ratio	11.28%	12.77%
II mode	Target damping ratio	10.00%	Estimated damping ratio	8.92%	10.79%

Table 1a: *Example of estimated mode shapes, frequencies and damping ratios for a two-storey frame, random input (targeted damping ratio 10%).*

Three-storey frame – Random input (ζ_k = 10%)					Δ% - MAC
I mode	Target frequency	2.650 Hz	Estimated frequency	2.658 Hz	0.30%
II mode	Target frequency	7.450 Hz	Estimated frequency	7.363 Hz	1.17%
III mode	Target frequency	10.76 Hz	Estimated frequency	10.44 Hz	2.97%
I mode	Target mode shape	0.3280 0.5910 0.7370	Estimated mode shape	0.3343 0.5890 0.7357	1.000
II mode	Target mode shape	-0.7370 -0.3280 0.5910	Estimated mode shape	-0.7323 -0.2804 0.6205	0.998
III mode	Target mode shape	0.5910 -0.7370 0.3280	Estimated mode shape	0.6345 -0.6999 0.3291	0.997
I mode	Target damping ratio	10.00%	Estimated damping ratio	10.76%	7.62%
II mode	Target damping ratio	10.00%	Estimated damping ratio	10.33%	3.28%
III mode	Target damping ratio	10.00%	Estimated damping ratio	10.48%	4.84%

Table 1b: *Example of estimated mode shapes, frequencies and damping ratios for a three-storey frame, random input (targeted damping ratio 10%).*

PART II: Modal identification with seismic response signals

5. Modal identification at seismic input on ideal frames

The algorithm's efficiency is further assessed by trials with seismic input, a type of signal that shall not fit among those strictly eligible for FDD identification. At this stage, high values of modal damping ratio have been also considered. Analyses have been performed through the developed refined FDD algorithm. Frames are subjected to three seismic excitations, applied at the base of the structures as SDOF ground acceleration:

- *El Centro Earthquake* (Imperial Valley, California, 18 May 1940): Magnitude M = 7.1, USGS-NSMP Station 0117 - NS component, PGA = 306.5 cm^2/s = 0.312 g, Length of registration t = 40 s, Sampling frequency f_s = 100 Hz;
- *L'Aquila Earthquake* (Abruzzo, Italy, 6 April 2009): Magnitude M = 5.8, AQV Station - WE component, PGA = 646.1 cm^2/s = 0.659 g, Length of registration t = 100 s, Sampling frequency f_s = 200 Hz;
- *Tohoku Earthquake* (Miyagi, Japan, 11 March 2011): Magnitude M = 9.0, MYG004 Station - NS component, PGA = 2647.8 cm^2/s = 2.699 g, Length of registration t = 300 s, Sampling frequency f_s = 100 Hz.

These seismic excitations are characterized by narrow frequency spectra and high energy content. Also, they are characterized by short and strictly non-stationary records. Following Fig. 5 represents the frequency content of the adopted earthquakes by the Fourier amplitude spectrum. Strong motion data are considered since they may affect the modal response and may bring to difficult modal parameter estimates [25], [26], [23], [14], [15]. Anyway, the developed algorithm, with its refined computational strategies, leads to effective estimates.

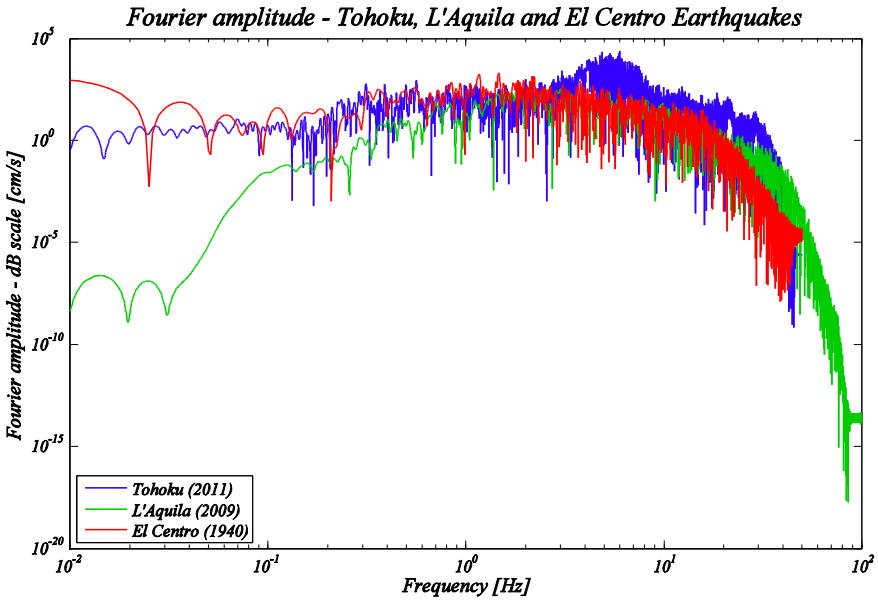

Figure 5: *Fourier amplitude spectra of the three adopted seismic excitations.*

5.1 FDD technique for seismic response signals and heavy damping

This paragraph presents some original theoretical considerations and explanations about the current use of strong ground motions with the implemented refined FDD technique. It explains why this rFDD algorithm works fairly well also at seismic input and concomitant heavy damping.

Unlike the PSD of white noise input (that runs-out approximately constant at every frequency instance of the spectrum), the PSD of an earthquake excitation changes with time and frequency [23]. Otherwise, in most cases it changes slowly over the frequency range, especially for an interval that is adequately wide to include the structural modal frequencies. In these cases the spectrum can be

considered sufficiently flat to approximate the trend of a white noise excitation with good accuracy, as it occurs for the set of adopted seismic excitations. These changes may be gradual enough to not significantly affect any individual modal peak of the structure. So, the ground motion would still generally be adopted as the broad-banded white noise input characteristic of OMA. This assertion may be illustrated in following Fig. 6, where, over the frequency range between 0 Hz and 15 Hz, interval containing all the examined structural modal frequencies, a linear interpolation is represented, proving through its slight angular coefficient the fairness of the present assumption.

As stated in previous Section 2.1, the FDD method relies on the assumption of stationary zero-mean white noise input, which implies that the input PSD matrix $\mathbf{G}_{xx}(\omega)$ is constant, hypothesis which is critical in the simplifications made in Eqs. (2.3) and (2.5). For some selected non-white noise input, as the previously-exposed ground motions, it is possible, within a good approximation, to ignore the frequency dependence of the input PSD matrix for a specific frequency interval, i.e. for a subset $\omega_{\text{Sub}} = \text{Sub}(\omega) \in \omega \Rightarrow f_{\text{Sub}} = \text{Sub}(f) \in f$, as the following:

$$\omega_{\text{Sub}} = \text{Sub}(\omega) = 2\pi f_{\text{Sub}} = 2\pi \text{Sub}(f)$$
$$\Rightarrow f_{\text{Sub}} = \text{Sub}(f) = \left[0,\ \frac{f_{\text{Nyq}}}{2\text{m}} = \frac{f_{\text{s}}}{4\text{m}}\right] \in f = [0,\ f_{\text{s}}] = \left[0,\ 2f_{\text{Nyq}} = f_{\text{s}}\right] \tag{5.1}$$

where $f_{\text{Nyq}} = f_{\text{s}}/2$ is the Nyquist frequency, f_{s} is the adopted sampling frequency and m is a positive integer which delineates the subinterval of frequencies. This work demonstrates that this assumption (and related simplification) leads to effective modal parameter estimates, taking also into account the peculiarities of the seismic excitations.

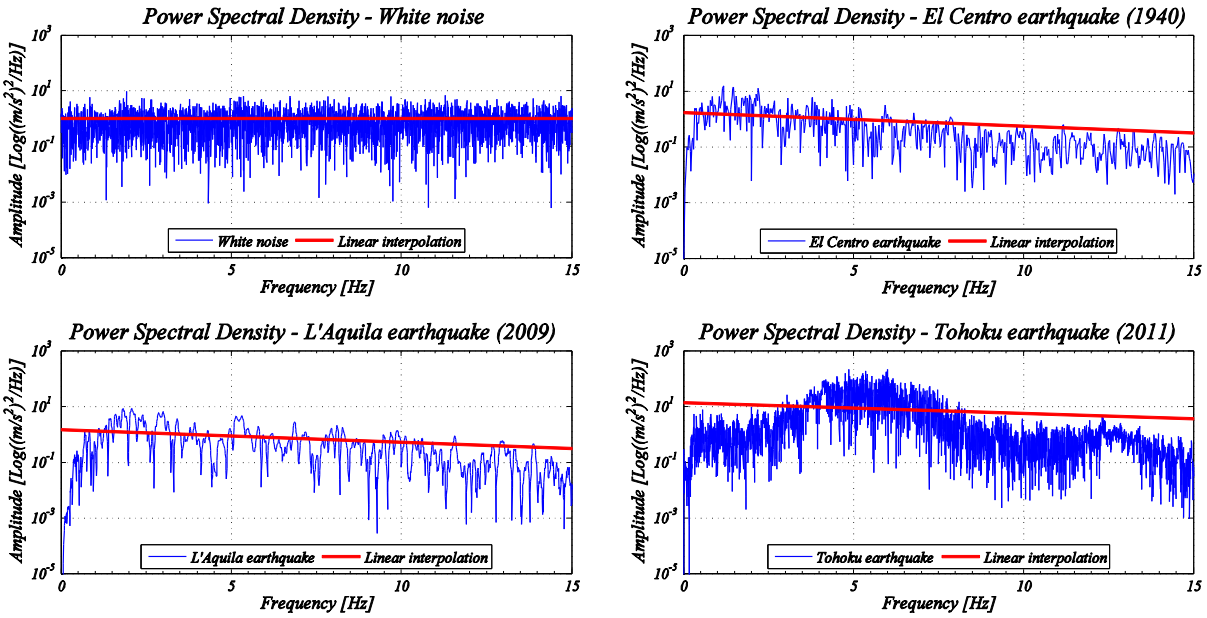

Figure 6: *Auto-Power Spectral Density of the adopted structural input excitations with related linear interpolation in the frequency range between 0 and 15 Hz.*

The developed refined FDD algorithm considers, among other strategies, the feature of defining $\mathbf{G}_{xx}(\omega_{\text{Sub}}) \Rightarrow \text{G}_{xx} = \overline{\text{G}}_{xx}$ for an interval $\omega_{\text{Sub}} = \text{Sub}(\omega) \in \omega$. Remembering Eq. (2.3), it is therefore possible to obtain:

$$\mathbf{G}_{yy}(\omega_{\text{Sub}}) \simeq \sum_{k=1}^{n}\sum_{s=1}^{n}\left(\frac{\overline{\mathbf{R}}_k \text{G}_{xx}}{-i\omega - \overline{\lambda}_k} + \frac{\mathbf{R}_k \text{G}_{xx}}{-i\omega - \lambda_k}\right)\left(\frac{\mathbf{R}_s^{\text{T}}}{i\omega - \lambda_s} + \frac{\mathbf{R}_s^{\text{H}}}{i\omega - \overline{\lambda}_s}\right) \tag{5.2}$$

Thus, all equations from (2.4) to (2.9) are still valid, recalling the approximation due to the use of the $\text{Sub}(\omega)$ interval.

Finally, it is possible to extract reliable estimates also at concomitant heavy damping. Especially, although theoretical derivations belong to the assumption of light damping, the algorithm may be applied to identify heavy damping. The hypothesis of lightly-damped structures has been made in Eq. (2.6), where the pole can be anyway expressed as $\lambda_k = -\zeta_k\omega_k + i\omega_{dk} \cong -\zeta_k\omega_k + i\omega_k$ even with heavy damping. In fact, by assuming a modal damping ratio ζ_k = 10%, the former equation carries to an error of about $5 \cdot 10^{-3}$ on the ω_{dk} computation (with respect to $5 \cdot 10^{-5}$ arising from ζ_k = 1%), an acceptable value in engineering terms. Accordingly, relations from Eq. (2.6) to Eq. (2.9) work properly, proving the theoretical effectiveness of the algorithm at heavy damping. With respect to the subsequent procedures for heavy damping estimates, theoretical derivations are still fully valid. Flattening of the peaks and extremely noisy SVs lead to critical conditions for classical EFDD procedures. The developed algorithm, with its procedures and strategies, described both in earlier Section 2.2 and Section 5.2 below, returns well-defined peaks and SVs, leading to effective modal parameter estimates, as it can be appreciated from the illustrative results provided in the paper. In particular, dealing with heavy damping, the iterative procedure should be adjusted in certain steps, namely: the MAC confidence level is set first to 0.8, and the extrema of the ACF ranging from 95% to 15% of its maximum amplitude are selected within the regression time window, allowing to speed up the iterative algorithm convergence.

5.2 Application of the refined FDD algorithm with SDOF seismic response input

In this section, comprehensive results at seismic input and heavy damping are reported, considering the analyzed two-, three- and six-storey shear-type frames, which modal damping ratios are taken from 1% to 5% and up (until 10% in some cases). Moreover, original strategies and arrangements adopted for the modal identification procedures are thoroughly exposed.

As experienced previously, for random input the SVD peak individuation may be possible by working on the first singular value, which contains already all the necessary information for achieving consistent estimates. The modal information is included also in subsequent SVs. It is very common that resonance peaks are located in the second or even in the third SV plot, but these are not generally employed to prevent noise occurrence in the results. This feature no longer holds at seismic input (characterized by non-stationary frequency spectra): the use of subsequent SVs becomes necessary to capture the modal peaks, although it may bring noise in the results. The use of seismic input and heavy damping leads to very noisy SVs representations, which often make unsuitable subsequent SVs. However, the developed algorithm improves the use of lower SVs with respect to traditional FDD, reducing disturbances and producing less noisy SVs, as it can be appreciated in Figs. 7a, 8a. The estimate of modal parameters is feasible by operating on different SVs at the same time. Through the Wiener-Khinchin procedure, a substantial help in the location of the correct resonance peaks is provided [34]. All results concerning the SVs in this work are represented with this procedure. Otherwise, the developed algorithm can estimate the PSD matrix also by the use of the classical Welch Modified Periodogram [35], as opportunely set, via the integrated procedure adopted by the rFDD algorithm. Then, the described methods globally lead to better modal parameter estimates. Moreover, the use of the SV product plot is complementary [14].

The PSD matrix, computed at each frequency line of the spectrum, fulfills all the required properties for the correct working of the FDD technique, despite the characteristics of the earthquake signals. Then, real diagonal terms and complex conjugate off-diagonal entries are provided, correspondingly to a Hermitian PSD matrix. Accordingly, the related phase angles are always zero on the diagonal and display a 180° shift outside. Additional results and comments on that are available in [34].

The filtering of data before modal identification (i.e. filtering of the simulated responses adopted then as input channels for the refined FDD algorithm) is now necessary, with respect to the use of random excitation, to leave-out undesired frequency contents, that for civil structures correspond to the high frequency components of the spectra. This portion of the spectra may be significant with earthquakes, and might be reduced or removed by an adequate low-pass filtering of the acquisitions. Estimates take quite a significant advantage from this feature. Also, the other procedures related to the refined FDD algorithm reported in Sections 2.2 and 2.3 help in improving the achieved estimates of the modal parameters.

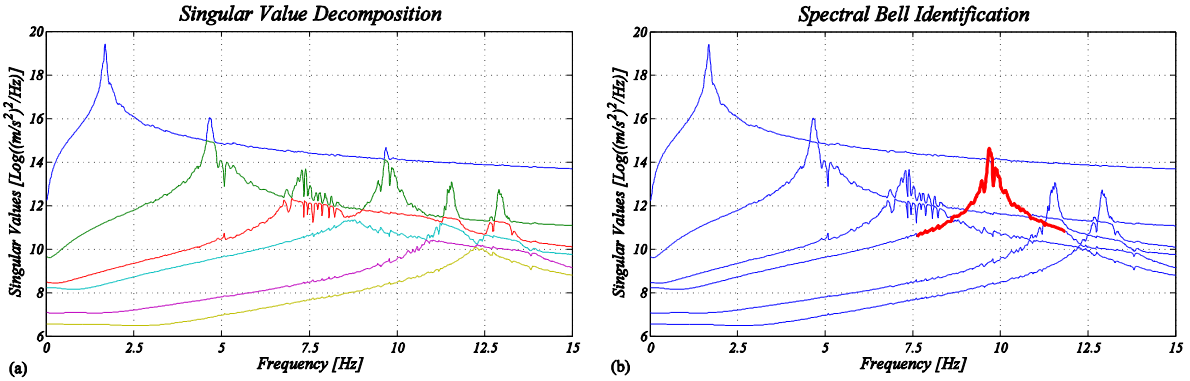

Figures 7a, 7b: *Display of the SVD and of the fictitious SV related to the fourth vibration mode, six-storey frame, L'Aquila earthquake.*

In case of very noisy SVs (e.g. especially with heavy damping), it is also possible to use appropriate computational strategies, associated to the standard SVD computation procedure. A partial overlapping of SVs is also possible. The individuation of spectral bells can be originally made as an envelope composition of different SVs portions, similarly to the common overlapping technique [40], by building a fictitious SDOF SV, as it is shown in Fig. 7b. In this case the spectral bell related to the fourth mode of vibration is composed as a fictitious SV from portions of different SVs (in this case the I, II, III and IV modes are adopted). Also, the peaks related to the III, V and VI modes can be found on the second SV curve, and the spectral bells can be similarly composed. This feature differs from the chance offered by classical EFDD algorithms, which allow the overlapping of SVs based upon the use of a modal peak positioned on the first SV. The presence of resonance peaks on different SVs may produce severe working conditions for traditional EFDD algorithms, which are supported here by the strategies of the current refined FDD procedure [14], [15].

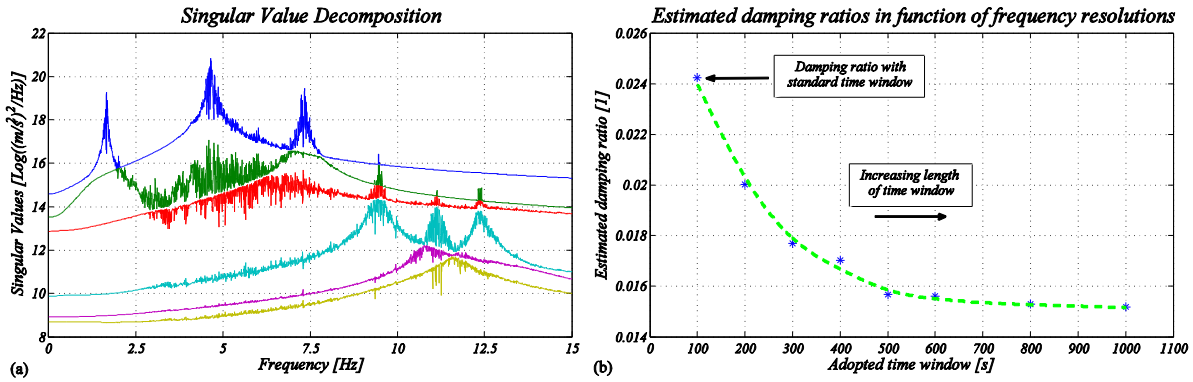

Figures 8a, 8b: *Display of the SVD, six-storey frame, Tohoku earthquake; comparison between estimated damping ratios as a function of frequency resolution, six-storey frame, L'Aquila earthquake.*

Another important issue concerns the frequency resolution. Seismic input signals display very limited registrations with respect to ambient recordings, and this may reduce the frequency resolution adopted for the PSD matrix evaluation. The use of a correct frequency resolution during computations affects directly the number of points which can be used during linear regression operations (and consequently the reliability of results) [15]. Also the other modal estimates are affected by the adopted frequency resolution [34]. Especially with short structural recordings (e.g. acquisitions derived from earthquakes), the frequency resolution might be enhanced by increasing the number of points used for the PSD matrix computations. To avoid the lacking of frequency resolution, this number of points has been increased by adding a zero-solicitation time window at the end of the earthquake recordings, thus increasing the record lengths with an operation that is known as zero-padding in classical signal analysis [33]. This issue is fundamental to reach effective modal parameter estimates, especially for the modal damping ratios [14]. Mainly, this operation must be performed for the low damping cases,

as it is possible to be appreciated in Fig. 8b, where a practical example is shown. Some analyses have been done as well to relate frequency resolution, record lengths and consistency of the estimates. There, a time window of 100 s corresponds to a frequency resolution of 0.01 Hz, while a time window of 1000 s corresponds to a frequency resolution of 0.001 Hz. Also the estimates of the remaining modal parameters (i.e. natural frequencies and mode shapes) are coherently improved [34].

Taking into account that the sampling frequency depends on the seismic registration and that the length of the time series can be extended as required to enhance the frequency resolution and therefore the estimates, the adopted parameters of the processing are the following:

- *Two-storey frame:* Length of time series $t = 400$ s, Sampling frequency $f_s = 100 - 200$ Hz (depending on the used earthquake), Adopted Frequency resolution $\Delta f = 0.0025$ Hz;
- *Three-storey frame:* Length of time series $t = 600$ s, Sampling frequency $f_s = 100 - 200$ Hz, Adopted Frequency resolution $\Delta f = 0.00167$ Hz;
- *Six-storey frame:* Length of time series $t = 1000$ s, Sampling frequency $f_s = 100 - 200$ Hz, Adopted Frequency resolution $\Delta f = 0.001$ Hz.

The two-, three- and six-storey frames were newly analyzed, under seismic excitation at the base. Modal damping ratios varying from 1% to 10% have been considered again. Results turn-out again very much consistent, even with heavy damping. Samples can be seen in Figs. 9-17, where El Centro, L'Aquila and Tohoku seismic excitations are considered in the presentation. For the two-storey and the three-storey cases the estimated mode shapes are always very accurate. The six-storey cases present still very good results, with MAC indexes which are always higher than 0.90 for the first three mode shapes. Only for the last eigenvectors, i.e. the fifth and sixth, the estimates are slightly less accurate than for the other cases, but anyway acceptable. This fact mainly depends on the very low effective modal mass associated to these modes, which leads to a small energy content in the SVs. The estimates may become less accurate, but still acceptable, with MAC indexes that are never below 0.7.

Two-storey frame at seismic input						
Target parameters	**I mode, f**	**II mode, f**	**I mode, ϕ**	**II mode, ϕ**	**I mode, ζ**	**II mode, ζ**
	4.211 Hz	10.920 Hz	0.5176; 0.8557	-0.8557; 0.5176	-	-
El Centro Earthquake (targeted damping ratios ζ_I = ζ_{II} = 10%)						
Classical EFDD estimates	3.886 Hz Δ=7.69%	10.254 Hz Δ=6.09%	0.5144; 0.8575 MAC=1.000	-0.9651; 0.2617 MAC=0.924	8.495% Δ=15.05%	6.244% Δ=37.56%
Refined EFDD estimates	4.294 Hz Δ=2.01%	11.182 Hz Δ=2.39%	0.5132; 0.8583 MAC=1.000	-0.8566; 0.5199 MAC=1.000	9.917% Δ=0.83%	10.186% Δ=1.86%
L'Aquila Earthquake (targeted damping ratios ζ_I = 7%, ζ_{II} = 5%)						
Classical EFDD estimates	4.346 Hz Δ=3.23%	10.614 Hz Δ=2.80%	0.5143; 0.8576 MAC=1.000	-0.9867; 0.1626 MAC=0.862	4.963% Δ=29.10%	6.381% Δ=27.62%
Refined EFDD estimates	4.327 Hz Δ=2.78%	10.625 Hz Δ=2.70%	0.5160; 0.8566 MAC=1.000	-0.9087; 0.4174 MAC=0.987	6.717% Δ=4.04%	4.628% Δ=7.45%
Tohoku Earthquake (targeted damping ratios ζ_I = ζ_{II} = 5%)						
Classical EFDD estimates	4.191 Hz Δ=0.48%	10.535 Hz Δ=3.54%	0.5171; 0.8559 MAC=1.000	-0.9545; 0.2984 MAC=0.943	2.558% Δ=48.85%	6.981% Δ=39.61%
Refined EFDD estimates	4.204 Hz Δ=0.15%	10.562 Hz Δ=3.28%	0.5175; 0.8557 MAC=1.000	-0.8895; 0.4569 MAC=0.995	4.745% Δ=5.11%	5.268% Δ=5.35%

Table 2: *Comparison of estimated mode shapes, frequencies and damping ratios among traditional EFDD (present implementation) and refined EFDD, two-storey frame, seismic input.*

Frequencies are always estimated on peaks, with visible resonance ones, and deviations which are always less than 5% on average. Damping ratios are also estimated appropriately for all the considered cases, by showing an average deviation that is reasonably contained, about 10% on average, especially concerning low values of the target damping ratios.

Again, the developed algorithm noticeably provides better estimates as compared to those from a traditional EFDD implementation [18], [19], [17]. This classical method has been implemented as well

into *MATLAB*, as it has been made for the present rFDD procedure, in order to compare the estimates between the two procedures and to achieve validation. Some comparison examples at seismic input and heavy damping are shown in Table 2, where the two-storey cases presented in following Figs. 9, 10, 11 are shown. The present refined FDD algorithm, clearly provides better estimates, especially for the modal damping ratios. Generally, for the traditional algorithm, MAC indexes are lower than 0.80 and sometimes the deviations of the natural frequency estimates run over 5%. Further, especially for the heavy-damped cases, the modal damping ratios estimates display deviations up to 30% for the first modes, while identification may fail for the higher modes.

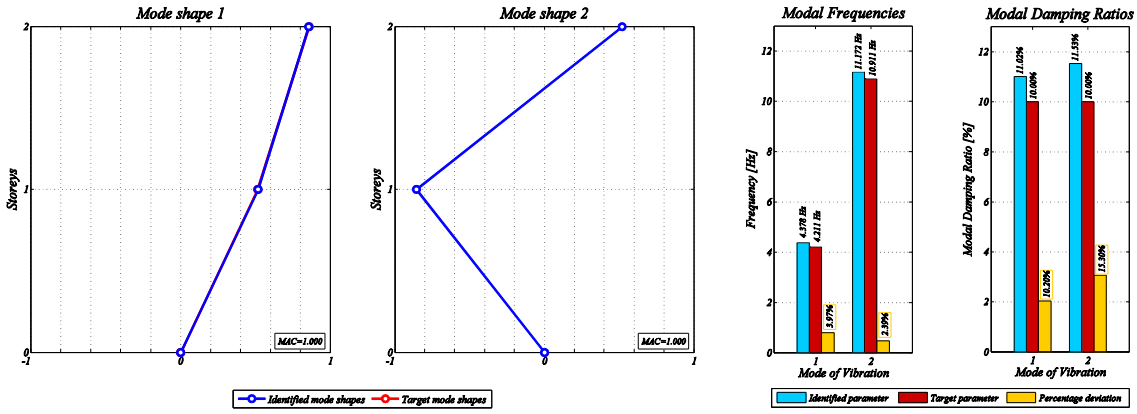

Figure 9: *Example of estimated mode shapes, frequencies and damping ratios for a two-storey frame, El Centro earthquake.*

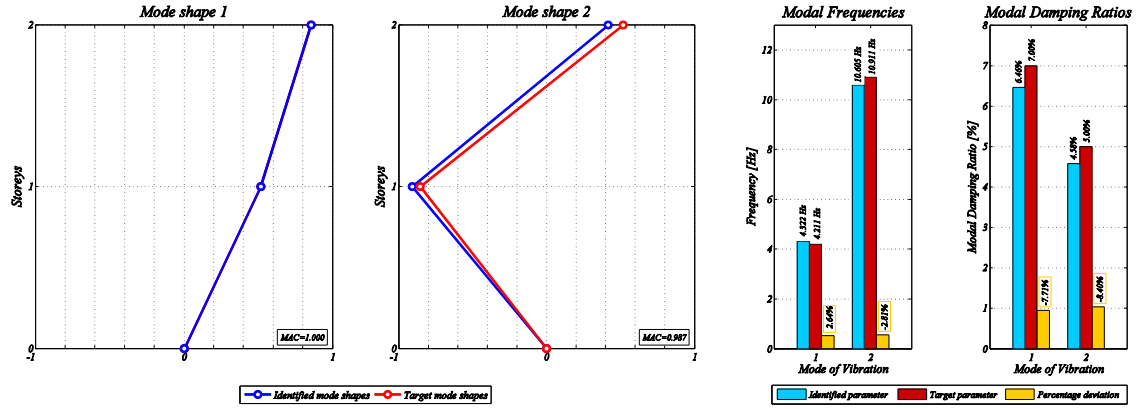

Figure 10: *Example of estimated mode shapes, frequencies and damping ratios for a two-storey frame, L'Aquila earthquake.*

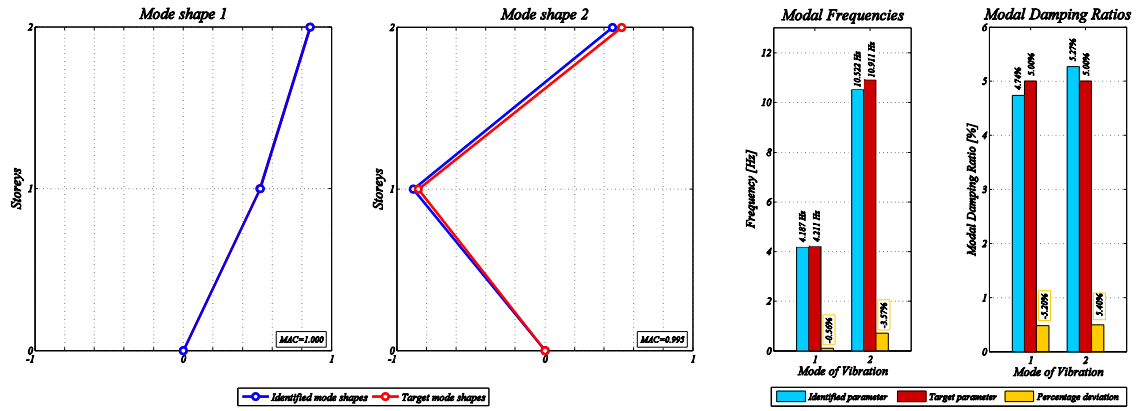

Figure 11: *Example of estimated mode shapes, frequencies and damping ratios for a two-storey frame, Tohoku earthquake.*

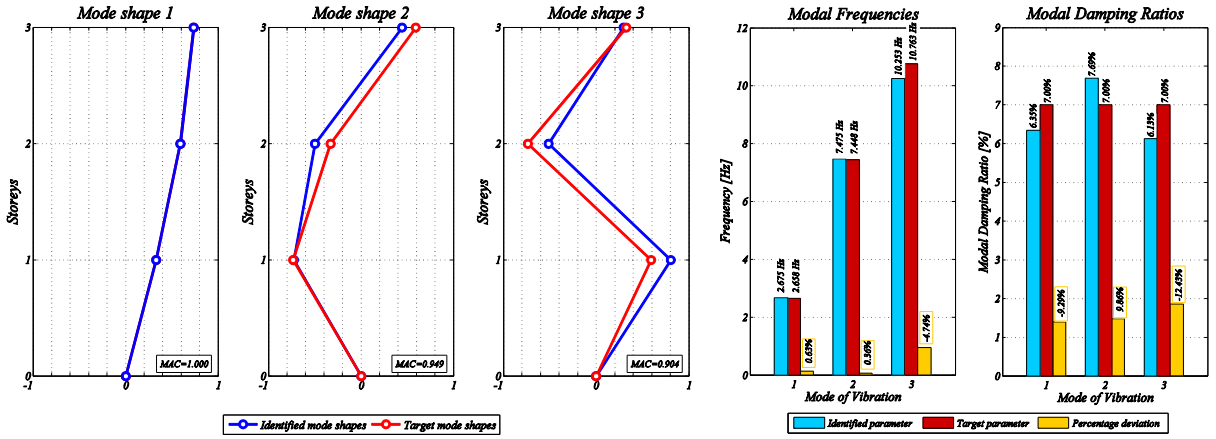

Figure 12: *Example of estimated mode shapes, frequencies and damping ratios for a three-storey frame, El Centro earthquake.*

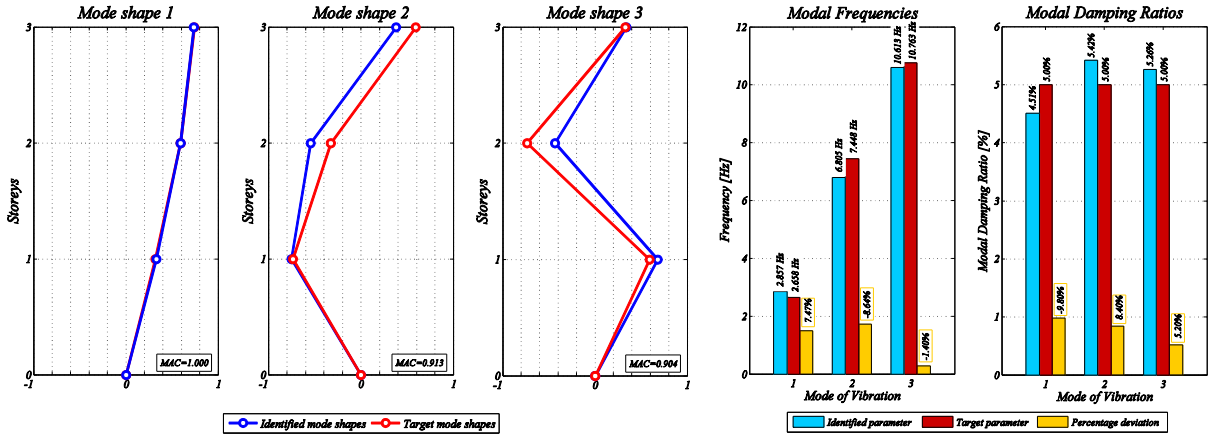

Figure 13: *Example of estimated mode shapes, frequencies and damping ratios for a three-storey frame, L'Aquila earthquake.*

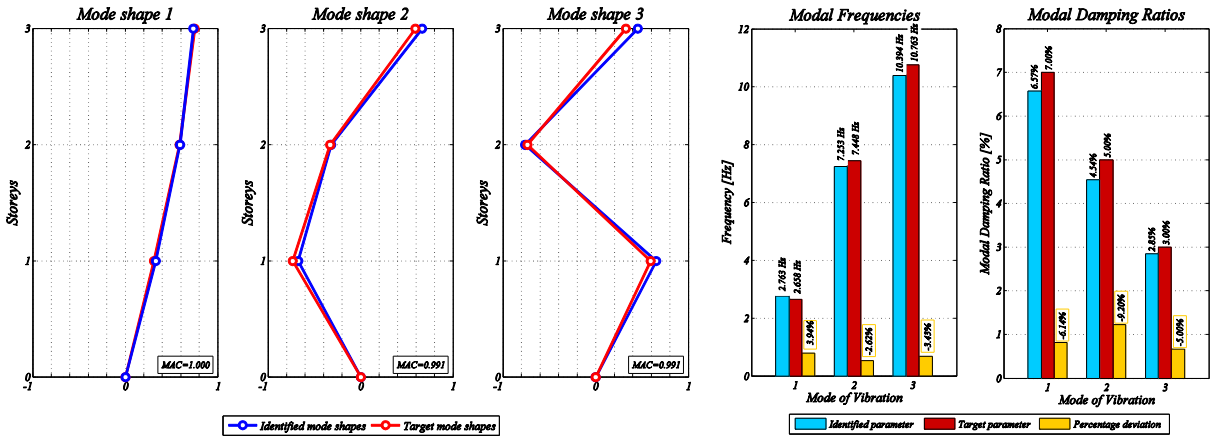

Figure 14: *Example of estimated mode shapes, frequencies and damping ratios for a three-storey frame, Tohoku earthquake.*

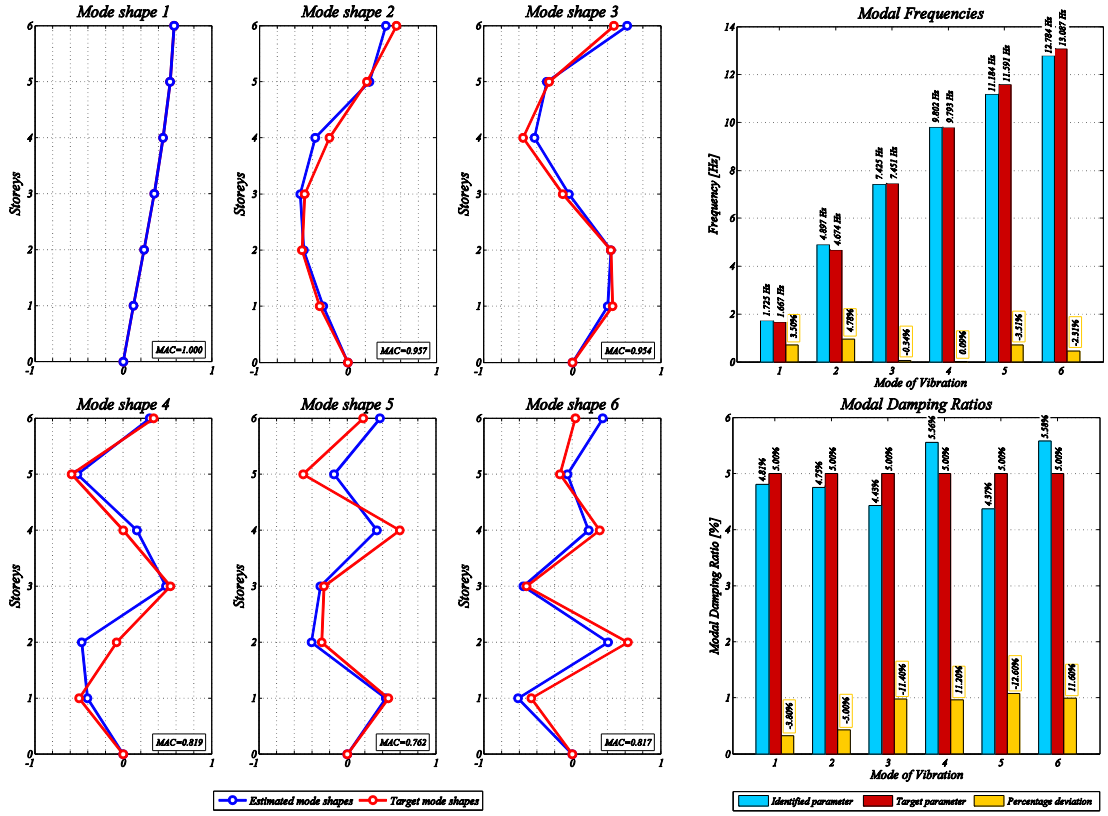

Figure 15: *Example of estimated mode shapes, frequencies and damping ratios for a six-storey frame, El Centro earthquake.*

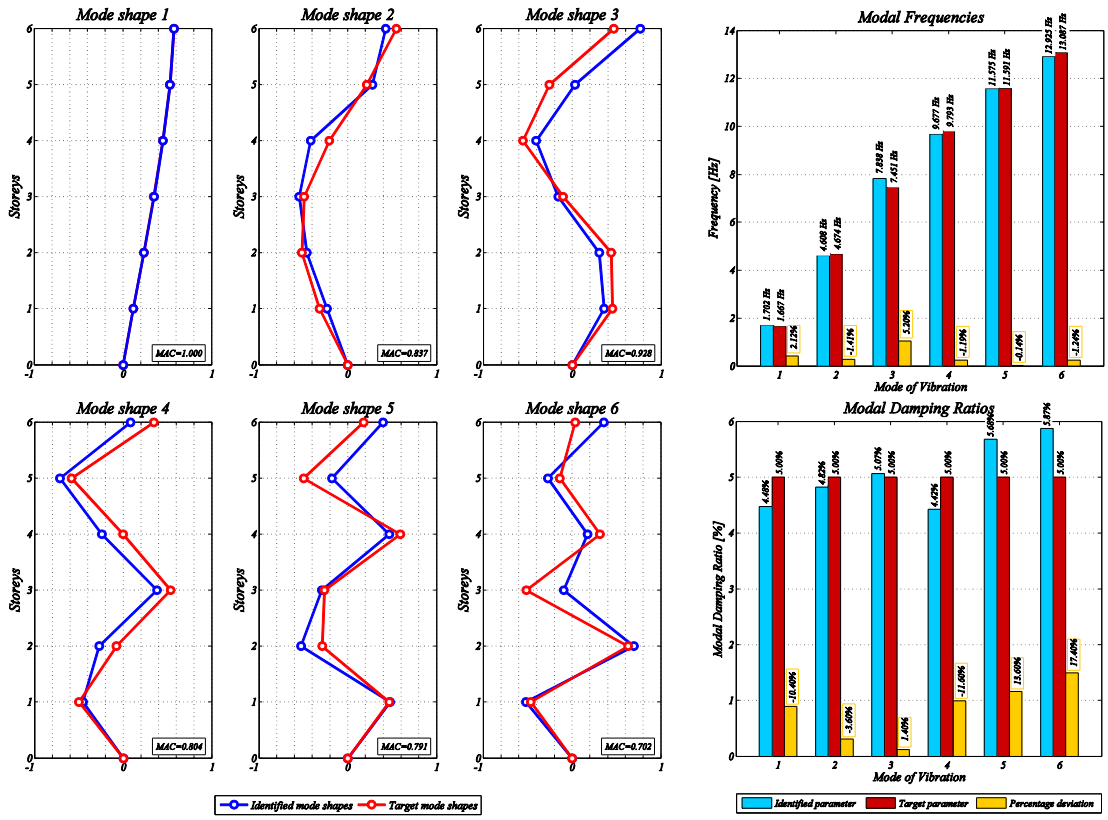

Figure 16: *Example of estimated mode shapes, frequencies and damping ratios for a six-storey frame, L'Aquila earthquake.*

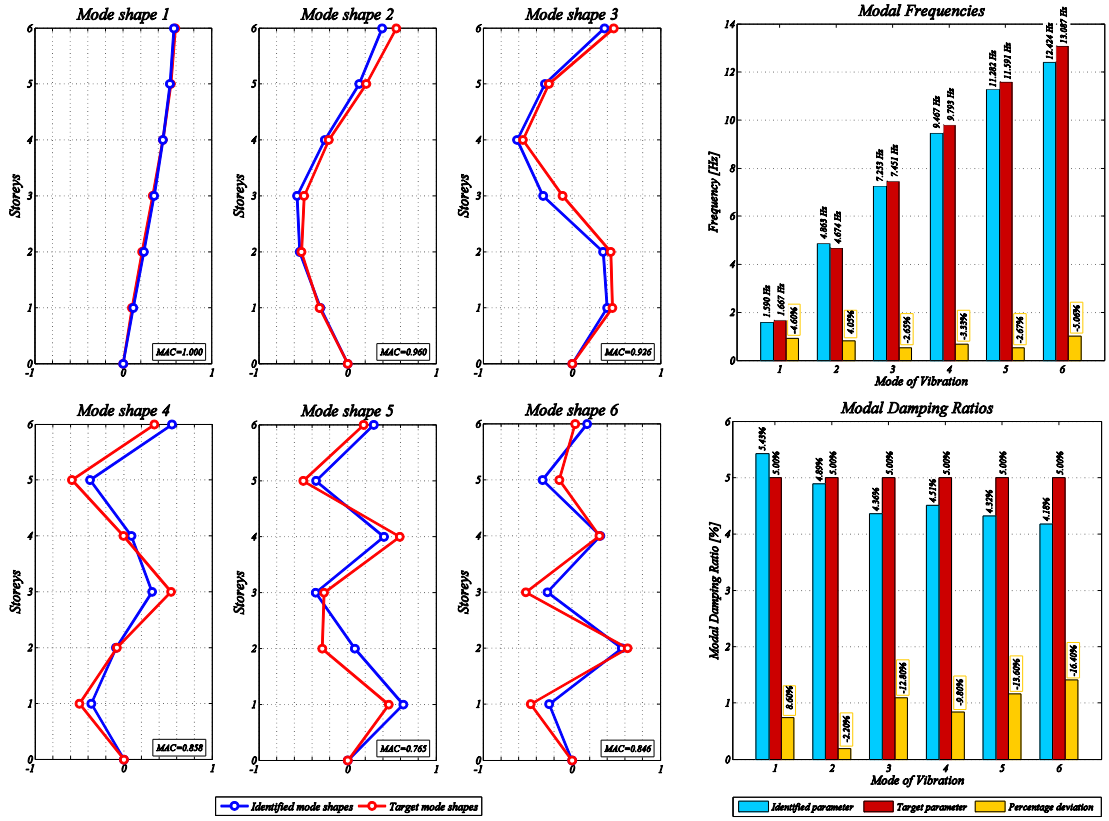

Figure 17: *Example of estimated mode shapes, frequencies and damping ratios for a six-storey frame, Tohoku earthquake.*

6. Modal identification of a realistic model structure with multiple seismic response input

Additionally to the previous results, further analyses concerning a realistic structure from the literature are presented in this section. These simulations are proposed to definitively validate the theoretical framework, even with more realistic cases, seeking to include all possible issues arising from real scenarios, i.e. close modes, heavy damping, multiple input ground motions, different locations of earthquakes and noise addition.

The taken testbed is a realistic ten-storey RC frame from the work of Villaverde and Koyama [41]. Main features of this structure may be found in Appendix B. This building is characterized by very close modes (the ten vibration modes are grouped into a 5 Hz frequency interval), while modal damping ratios are taken here according to a classical Rayleigh's damping approach, i.e. by a linear combination of stiffness and mass matrices. In particular, ζ_k for the first two modes are taken as 2% and 2.5%, determining consequently damping ratios up to 9%, for the last mode of vibration. Similar damping ratios represent very well the scenario from a real RC building, leading to very high values to be estimated with an OMA procedure. Furthermore, attempts with ζ_k = 2% and with ζ_k= 5% taken constant for all the modes are performed as well, confirming the goodness of the developed algorithm. For the present implementation only selected results are presented, see the following subsections.

6.1 Multiple input earthquake components

Although the methodology deals with an output-only scenario, in terms of real seismic engineering implications, multiple input ground motions are considered for validation too. These derive from different recording directions of the adopted seismic records, i.e. as combinations of the horizontal components of the seismic action, as suggested by Eurocode 8 (see UNI EN 1998-1:2004, Par. 4.3.3.5.1). Accordingly, the action effects due to the combination of the horizontal components of the seismic excitation may be computed using both the following two combinations, i.e.

E_{Edx} " + " 0.30 E_{Edy} and 0.30 E_{Edx} " + " E_{Edy}, where " + " implies "to be combined with", E_{Edx} and E_{Edy} represent the action effects due to the application of the earthquake motion along the x and y axis of the structure, respectively. In this way, four combinations of seismic actions are considered, taking into account their possible directions, namely:

- Comb. 1: $E_{NS} + 0.30\ E_{WE}$;
- Comb. 2: $E_{NS} - 0.30\ E_{WE}$;
- Comb. 3: $0.30\ E_{NS} + E_{WE}$;
- Comb. 4: $0.30\ E_{NS} - E_{WE}$.

These combinations are taken into account and analyzed for each considered earthquake, i.e. the same strong ground motions as in the previous analysis, except that now both NS and WE components are adopted. Forthcoming Table 3 reports the characteristics of the adopted ground motions. For all the analyses, time series of a 400 s length and 0.0025 Hz frequency resolution have been adopted.

Earthquake	Date	Station	Duration [s]	f_s [Hz]	M	Comp.	PGA [g]
El Centro	18/05/1940	0117	40	100	7.1	NS	0.312
						WE	0.214
L'Aquila	06/04/2009	AQV	100	200	5.8	NS	0.546
						WE	0.659
Tohoku	11/03/2011	MYG004	300	100	9.0	NS	2.699
						WE	1.268

Table 3: *Main characteristics of the adopted set of earthquakes for the multiple input analysis of the ten-storey frame.*

The following Fig. 18 represents the SVD and the normalized ACF curve fitting procedure for the fifth mode of vibration of the ten-storey frame subjected to L'Aquila earthquake, NS component. Then, subsequent Table 4 summarizes some results achieved from the use of L'Aquila earthquake (NS and WE components), jointly with the multiple input ground motions outlined by the previous four combinations.

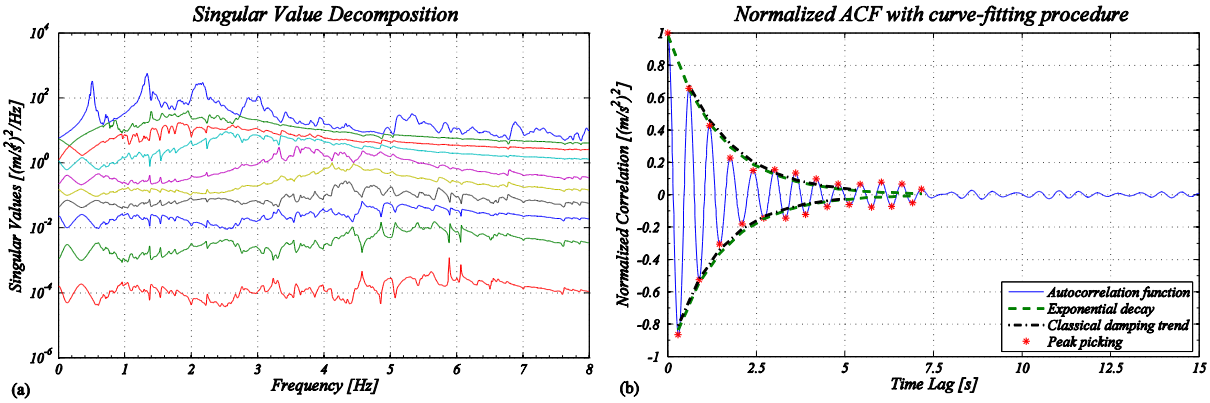

Figures 18a, 18b: *Display of the SVD and of the normalized ACF curve fitting procedure for the fifth mode of vibration, ten-storey frame, L'Aquila earthquake, NS component.*

It is possible to appreciate that the identified natural frequencies display deviations that are less than 5% for every case, with mean values less than 2.3% on average, while modal damping ratios display deviations that are less than 20%, with mean values less than 9.2% on average. Noticeable looks the fact that though the modal damping ratios assume high values at increasing mode number, the rFDD algorithm keeps working very well, proving once again its full effectiveness also in real earthquake applications. The identified mode shapes, finally, display MAC indexes always greater than 0.85 for the first three modes, while they slightly decrease for the fourth and fifth modes. Mode shapes for modes above the fifth, until the tenth, display poor values of the MAC index, thus these values have not been reported in the table.

An explanation about the effective estimates related to natural frequencies and damping ratios for all the modes, while mode shapes goodness decreases after the fifth eigenvector, could be sought through

an investigation on the effective modal masses. In fact, the first three modes take the 96% of the effective modal mass associated to the frame, while the fourth and fifth modes display only the 3% of the total mass and the remaining 1% is distributed on the last five modes. This means that, equivalently, the energy content brought by the modes, and then by the signal itself, is wider relating to the first three modes of vibration, and rapidly decreases for the subsequent modes. Consequently, the information carried by the SVs suffers from a deterioration of quality, determining poor values of the last MAC indexes, since the mode shapes are the most difficult parameters to be estimated, especially at seismic input and at heavy damping (due to non-stationarity of the input, which jointly with heavy damping leads to very noisy SVs). Anyway, these results shall be considered excellent in engineering terms, proving again the effectiveness of the developed algorithm.

Then, Figs. 19-21 underline the estimates obtained by all the performed analyses, showing the maximum and minimum deviations related to the natural frequencies and modal damping ratios, for each mode of vibration and for each adopted set of earthquakes (i.e. grouped results for El Centro, L'Aquila and Tohoku ground motions). Similarly, Fig. 22 represents the minimum and maximum deviations, for the whole adopted earthquakes.

Mode		f_{TARG} ζ_{TARG}	AQ - NS comp. -	AQ - WE comp. -	AQ - Comb. 1 -	AQ - Comb. 2 -	AQ - Comb 3 -	AQ - Comb. 4 -
1	**f [Hz]** **ζ[%]**	0.500 2.00 -	0.518 - Δ=3.44% 2.05 - Δ=2.46% MAC=1.000	0.508 - Δ=1.48% 1.96 - Δ=2.04% MAC=1.000	0.508 - Δ=1.48% 1.95 - Δ=2.43% MAC=1.000	0.508 - Δ=1.48% 2.05 - Δ=2.29% MAC=1.000	0.508 - Δ=1.48% 2.15 - Δ=7.63% MAC=1.000	0.508 - Δ=1.48% 2.05 - Δ=2.40% MAC=1.000
2	**f [Hz]** **ζ[%]**	1.326 2.50 -	1.338 - Δ=0.87% 2.59 - Δ=3.49% MAC=0.999	1.338 - Δ=0.87% 2.59 - Δ=3.59% MAC=0.999	1.338 - Δ=0.87% 2.39 - Δ=4.52% MAC=0.999	1.338 - Δ=0.87% 2.39 - Δ=4.32% MAC=0.999	1.338 - Δ=0.87% 2.51 - Δ=0.30% MAC=0.999	1.328 - Δ=0.14% 2.66 - Δ=6.36% MAC=0.998
3	**f [Hz]** **ζ[%]**	2.151 3.59 -	2.178- Δ=1.23% 3.35 - Δ=6.60% MAC=0.979	2.099 - Δ=2.40% 3.71 - Δ=3.30% MAC=0.890	2.148 - Δ=0.13% 3.68 - Δ=2.40% MAC=0.987	2.178 - Δ=1.23% 3.26 - Δ=9.27% MAC=0.983	2.109 - Δ=1.94% 3.69 - Δ=2.76% MAC=0.910	2.099 - Δ=2.40% 3.22 - Δ=10.30% MAC=0.889
4	**f [Hz]** **ζ[%]**	2.934 4.71 -	3.008 - Δ=2.52% 4.17 - Δ=11.49% MAC=0.810	3.008 - Δ=2.52% 4.84 - Δ=2.72% MAC=0.827	3.008 - Δ=2.52% 4.07 - Δ=13.67% MAC=0.827	2.881 - Δ=1.81% 4.48 - Δ=4.83% MAC=0.830	3.008 - Δ=2.52% 3.93 - Δ=16.38% MAC=0.827	2.891 - Δ=1.46% 4.51 - Δ=4.29% MAC=0.610
5	**f [Hz]** **ζ[%]**	3.653 5.77 -	3.633 - Δ=0.56% 5.63 - Δ=2.51% MAC=0.809	3.594 - Δ=1.63% 5.11 - Δ=11.40% MAC=0.799	3.633 - Δ=0.56% 5.55 - Δ=3.73% MAC=0.109	3.633 - Δ=0.86% 4.94 - Δ=14.46% MAC=0.835	3.594 - Δ=1.63% 5.89 - Δ=2.05% MAC=0.799	3.594 - Δ=1.63% 5.22 - Δ=9.49% MAC=0.799
6	**f [Hz]** **ζ[%]**	4.292 6.73 -	4.326 - Δ=0.80% 5.88 - Δ=12.66% -	4.375 - Δ=1.93% 6.47 - Δ=3.86% -	4.326 - Δ=0.80% 5.85 - Δ=13.14% -	4.326 - Δ=0.79% 6.31 - Δ=6.17% -	4.375 - Δ=1.93% 6.27 - Δ=6.84% -	4.102 - Δ=4.44% 6.19 - Δ=8.00% -
7	**f [Hz]** **ζ[%]**	4.836 7.55 -	4.707 - Δ=2.66% 7.60 - Δ=0.73% -	4.639 - Δ=4.07% 7.17 - Δ=5.07% -	4.756 - Δ=1.65% 6.62 - Δ=12.30% -	4.648 - Δ=3.87% 6.59 - Δ=12.68% -	4.834 - Δ=0.03% 7.90 - Δ=4.63% -	4.844 - Δ=0.17% 6.88 - Δ=8.85% -
8	**f [Hz]** **ζ[%]**	5.272 8.21 -	5.147 - Δ=2.37% 8.17 - Δ=0.43% -	5.205 - Δ=1.26% 7.61 - Δ=7.28% -	5.156 - Δ=2.19% 7.62 - Δ=7.14% -	5.147 - Δ=2.37% 7.44 - Δ=9.40% -	5.156 - Δ=2.19% 7.47 - Δ=9.06% -	5.205 - Δ=1.26% 7.03 - Δ=14.39% -
9	**f [Hz]** **ζ[%]**	5.591 8.69 -	5.322 - Δ=4.80% 8.67 - Δ=0.20% -	5.420 - Δ=3.05% 8.62 - Δ=0.76% -	5.322 - Δ=4.80% 8.18 - Δ=5.83% -	5.322 - Δ=4.80% 7.72 - Δ=11.20% -	5.381 - Δ=3.75% 7.92 - Δ=8.84% -	5.420 - Δ=3.05% 8.28 - Δ=4.76% -
10	**f [Hz]** **ζ[%]**	5.787 8.99 -	5.811 - Δ=0.41% 8.70 - Δ=3.18% -	5.732 - Δ=0.93% 9.16 - Δ=1.92% -	5.820 - Δ=0.58% 9.70 - Δ=7.89% -	5.762 - Δ=0.43% 8.04 - Δ=10.55% -	5.732 - Δ=0.93% 8.58 - Δ=4.56% -	5.732 - Δ=0.93% 9.28 - Δ=3.26% -

Table 4: *Example of estimated frequencies, modal damping ratios (ranging from 2% to 9%) and MAC indexes for the ten-storey frame, L'Aquila earthquake: NS, WE components and combinations for multi-component earthquakes.*

6.2 Multiple input earthquake locations

Another issue addressed with the present analysis is the consideration of different seismic input coming from various seismic signals recorded around a selected location. In fact, by validating the methodology with seismic excitations, the ground motion data fed to the simulation is not the actual system input, but only highly correlated to the structural input. In real earthquake engineering applications, the ground motion data collected at different locations will be way different, and none of those could be claimed as the pure input. So, while previously only a single earthquake record leading to peak shaking was considered (or multiple input ground motions, as before), on a single location, further results are produced by considering signals that come from different accelerometer recordings at nearby stations.

For these attempts, L'Aquila earthquake from different locations (i.e. from different recording stations) has been considered, adopting either the NS and the WE component. Subsequent Table 5 reports the characteristics of the adopted ground motions. All the stations with a record of at least 0.1 g PGA are selected. Above the classical information, also epicentral distance, Vs30 (shear wave velocity for the top 30 m of subsurface profile), site and morphological classifications (according to Eurocode 8) are reported. All records display a frequency sampling of 200 Hz. For all the analyses, time series of 400 s length and 0.0025 Hz frequency resolution have been adopted.

Station	Epic. Dist. [km]	Duration [s]	Vs30 [m/s]	Site	Morph.	Comp.	PGA [g]
AQA	5.2	100	552	B	V, T1	NS	0.442
						WE	0.402
AQG	5.1	100	685	B	S, T1	NS	0.489
						WE	0.446
AQK	1.8	100	717	B	S, T1	NS	0.353
						WE	0.330
AQU	2.4	90	-	C*	-, T1	NS	0.308
						WE	0.260
AQV	5.1	100	474	B	V, T1	NS	0.546
						WE	0.659
GSA	14.6	100	488	B	S, T1	NS	0.145
						WE	0.149

Table 5: *Main characteristics (according to Eurocode 8) of the adopted set of earthquakes from different locations, L'Aquila earthquake.*

Following Table 6 reports some results from the different L'Aquila seismic records, NS component. Again, the identified natural frequencies display deviations that are less than 5% for every case, with mean values that are less than 2.2% on average, while modal damping ratios display deviations that are less than 20%, with mean values that are less than 10.9% on average. The identified mode shapes, finally, display MAC indexes always greater than 0.95 for the first three modes, while they slightly decrease for the fourth and fifth modes. As before, mode shapes above the fifth, until the tenth, display poor values of the MAC index, thus are felt unreliable (see previous comments in Section 6.1 on the effective modal masses).

The achieved results are still optimal in engineering terms: Figs. 23 and 24 display the maximum and minimum deviations pertaining to natural frequencies and damping ratios, for each mode of vibration and for the set of L'Aquila seismic records, gathered for NS and WE components. Then, Fig. 25 represents the minimum and maximum deviations, for the overall earthquakes and components.

6.3 Issues of noise and attempts in real scenarios

Furthermore, notice that by feeding ground motion data into the Newmark method, the outcome could not be claimed as the pure output, since another relevant concern may be that of noise related to the data. This issue, i.e. the adding of noise to the recordings, looking for a closer representation of real conditions, has been widely explored within the present work. Especially, two conditions of noise addition are thoroughly studied, i.e. the addition of noise on pure earthquake records, before the application of the Newmark method, and on the achieved structural response, after the Newmark procedure. The first condition is adopted simply on the original seismic registration, while the second, more meaningful, is employed towards the possible presence of noise from instrumentations during the acquisition phases. In both cases, uncorrelated white Gaussian noise is added, in terms of percentage of power (in dB) of the original pure signal.

Analyzed cases include either multiple input earthquakes or ground motion data collected at different locations, as adopted before, jointly with heavy damping. The first case of noise addition is not truly meaningful for real identification purposes, since it does not lead to significant changes in the estimate procedures. Considerable is instead the second possibility: in the present work, some attempts have been performed, varying the power of the added noise from 0.01% to 10% of the power of the response signal. Until 0.5% no relevant changes are affecting the estimates, since all peaks are visible

and identifiable. Instead, varying the noise power from 1% to 5%, parameter identification becomes more challenging, but all peaks may be detected, with deviations of natural frequencies lower than 5% and slightly less accurate modal damping ratios, which display maximum deviations of 25%. The mode shapes are correctly estimated until the fourth peak, while the evaluations of the fifth mode shape get into troubles.

Mode		f_{TARG} ζ_{TARG}	AQA - NS comp. -	AQG - NS comp. -	AQK - NS Comp. -	AQU - NS Comp. -	AQV - NS Comp. -	GSA - NS Comp. -
1	**f [Hz]**	0.500	0.518 - Δ=3.44%	0.518 - Δ=3.44%	0.498 - Δ=0.48%	0.513 - Δ=2.46%	0.518 - Δ=3.44%	0.508 - Δ=1.48%
	ζ[%]	2.00	1.91 - Δ=4.58%	1.94 - Δ=2.87%	2.10 - Δ=5.15%	2.09 - Δ=4.30%	2.05 - Δ=2.46%	2.05 - Δ=2.58%
		-	MAC=1.000	MAC=1.000	MAC=1.000	MAC=1.000	MAC=1.000	MAC=1.000
2	**f [Hz]**	1.326	1.367 - Δ=3.08%	1.338 - Δ=0.87%	1.338 - Δ=0.87%	1.331 - Δ=0.32%	1.338 - Δ=0.87%	1.348 - Δ=1.61%
	ζ[%]	2.50	2.21 - Δ=11.43%	2.40 - Δ=3.94%	2.64 - Δ=5.68%	2.39 - Δ=4.44%	2.59 - Δ=3.49%	2.23 - Δ=10.63%
		-	MAC=0.976	MAC=0.999	MAC=0.999	MAC=0.999	MAC=0.999	MAC=0.997
3	**f [Hz]**	2.151	2.197- Δ=2.14%	2.119 - Δ=1.49%	2.148 - Δ=0.13%	2.185 - Δ=1.58%	2.178 - Δ=1.23%	2.158 - Δ=0.33%
	ζ[%]	3.59	2.99 - Δ=16.83%	3.01 - Δ=16.04%	3.18 - Δ=11.53%	3.54 - Δ=1.40%	3.35 - Δ=6.60%	3.18 - Δ=11.43%
		-	MAC=0.966	MAC=0.926	MAC=0.987	MAC=0.991	MAC=0.979	MAC=0.989
4	**f [Hz]**	2.934	2.881 - Δ=1.81%	2.822 - Δ=3.80%	2.891 - Δ=1.48%	2.930 - Δ=0.14%	3.008 - Δ=2.52%	2.959 - Δ=0.86%
	ζ[%]	4.71	4.14 - Δ=12.08%	4.46 - Δ=5.31%	4.15 - Δ=11.99%	4.50 - Δ=4.45%	4.17 - Δ=11.49%	4.12 - Δ=12.44%
		-	MAC=0.836	MAC=0.708	MAC=0.847	MAC=0.775	MAC=0.810	MAC=0.668
5	**f [Hz]**	3.653	3.711 - Δ=1.58%	3.682 - Δ=0.77%	3.711 - Δ=1.59%	3.748 - Δ=2.58%	3.633 - Δ=0.56%	3.516 - Δ=3.77%
	ζ[%]	5.77	4.97 - Δ=13.81%	5.48 - Δ=4.97%	5.41 - Δ=6.22%	5.30 - Δ=8.07%	5.63 - Δ=2.51%	5.48 - Δ=4.99%
		-	MAC=0.836	MAC=0.845	MAC=0.345	MAC=0.137	MAC=0.809	MAC=0.685
6	**f [Hz]**	4.292	4.092 - Δ=4.66%	4.404 - Δ=2.62%	4.356 - Δ=1.48%	4.138 - Δ=3.58%	4.326 - Δ=0.80%	4.297 - Δ=0.11%
	ζ[%]	6.73	5.79 - Δ=13.99%	6.16 - Δ=8.40%	5.98 - Δ=11.14%	5.77 - Δ=14.20%	5.88 - Δ=12.66%	5.99 - Δ=10.89%
		-	-	-	-	-	-	-
7	**f [Hz]**	4.836	4.766 - Δ=1.43%	4.902 - Δ=1.38%	4.805 - Δ=0.64%	4.871 - Δ=0.72%	4.707 - Δ=2.66%	4.668 - Δ=3.47%
	ζ[%]	7.55	6.09 - Δ=19.35%	6.91 - Δ=8.42%	6.33 - Δ=16.21%	6.57 - Δ=12.92%	7.60 - Δ=0.73%	6.40 - Δ=15.19%
		-	-	-	-	-	-	-
8	**f [Hz]**	5.272	5.166 - Δ=2.00%	5.205 - Δ=1.26%	5.078 - Δ=3.67%	5.273 - Δ=0.03%	5.147 - Δ=2.37%	5.215 - Δ=1.08%
	ζ[%]	8.21	7.89 - Δ=3.91%	7.41 - Δ=9.79%	7.59 - Δ=7.59%	7.47 - Δ=8.95%	8.17 - Δ=0.43%	7.89 - Δ=3.85%
		-	-	-	-	-	-	-
9	**f [Hz]**	5.591	5.440 - Δ=2.70%	5.410 - Δ=3.23%	5.518 - Δ=1.30%	5.554 - Δ=0.65%	5.322 - Δ=4.80%	5.547 - Δ=0.78%
	ζ[%]	8.69	8.23 - Δ=5.33%	8.10 - Δ=6.79%	8.07 - Δ=7.16%	8.10 - Δ=6.80%	8.67 - Δ=0.20%	8.04 - Δ=7.46%
		-	-	-	-	-	-	-
10	**f [Hz]**	5.787	5.723 - Δ=1.10%	6.007 - Δ=3.80%	5.742 - Δ=0.77%	6.018 - Δ=4.00%	5.811 - Δ=0.41%	5.820 - Δ=0.58%
	ζ[%]	8.99	8.62 - Δ=4.09%	8.59 - Δ=4.45%	8.72 - Δ=3.04%	8.73 - Δ=2.90%	8.70 - Δ=3.18%	9.14 - Δ=1.68%
		-	-	-	-	-	-	-

Table 6: *Example of estimated frequencies, modal damping ratios (ranging from 2% to 9%) and MAC indexes for the ten-storey frame, L'Aquila earthquake: NS component from different locations.*

Finally, setting a very high noise value equal to 10%, the last two to three modes become unidentifiable. Although, the remaining modes display once again very good estimates, showing deviations that are less than 5% for the natural frequencies and less than 25% for the modal damping ratios. Mode shapes are correctly estimated for the first three peaks; rather, the fourth peaks sometimes return poor values of the MAC index, as for the remaining identified modes. Finally, it is possible to prove the effectiveness of the algorithm also in the challenging cases where noise is added to the original signals, approaching even more the scenario of real earthquake response signals.

Concluding with the final validation of the algorithm at seismic input, analyses have been performed also by processing real earthquake response signals, i.e. real in-situ collected structural responses, as reported in [42]. The validation with synthetic signals produced here shall be considered as a necessary condition for validation with earthquake input (and also with heavy damping). Despite the increased difficulty in working with real data, it has been verified that the present procedure works well also with real earthquake response signals. This shall prove the rFDD effectiveness also for up-to-date detection of building properties in the earthquake engineering range.

In the case of real earthquake response input, the integrated approach for the PSD matrix evaluation and the iterative loop for the damping estimation become fundamental steps in order to achieve reliable modal estimates. A careful condition refers to the sampling frequency and the duration of the recordings, since the PSD matrix may be affected by slight inaccuracies. The accurate data filtering before identification looks also an essential step, in order to achieve effective modal parameter estimates at real earthquake input.

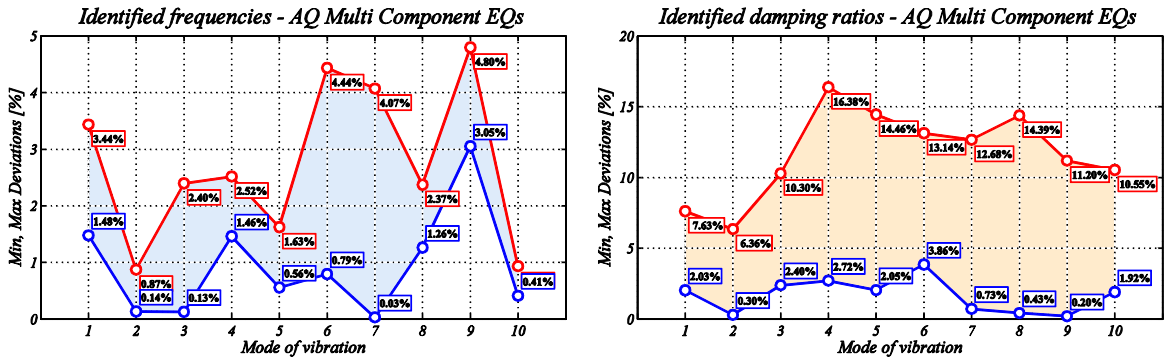

Figure 19: *Minimum and maximum deviations for identified frequencies and modal damping ratios (ranging from 2% to 9%), ten-storey frame, L'Aquila earthquake: multi-component earthquakes.*

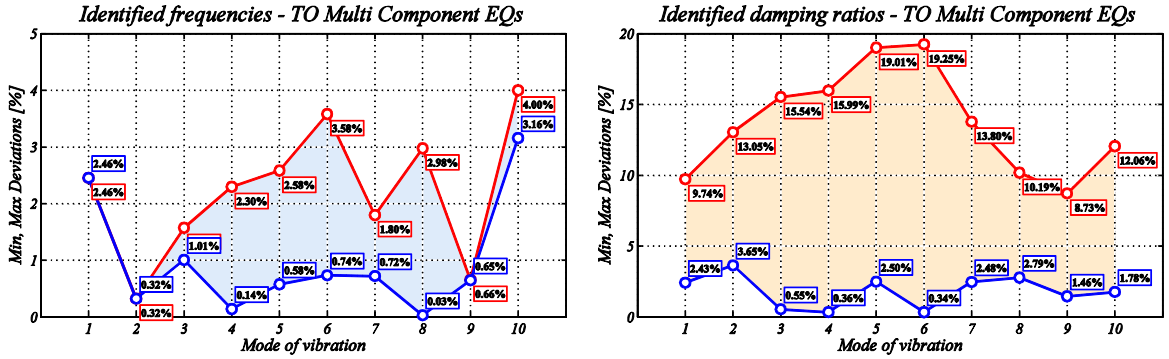

Figure 20: *Minimum and maximum deviations for identified frequencies and modal damping ratios (ranging from 2% to 9%), ten-storey frame, Tohoku earthquake: multi-component earthquakes.*

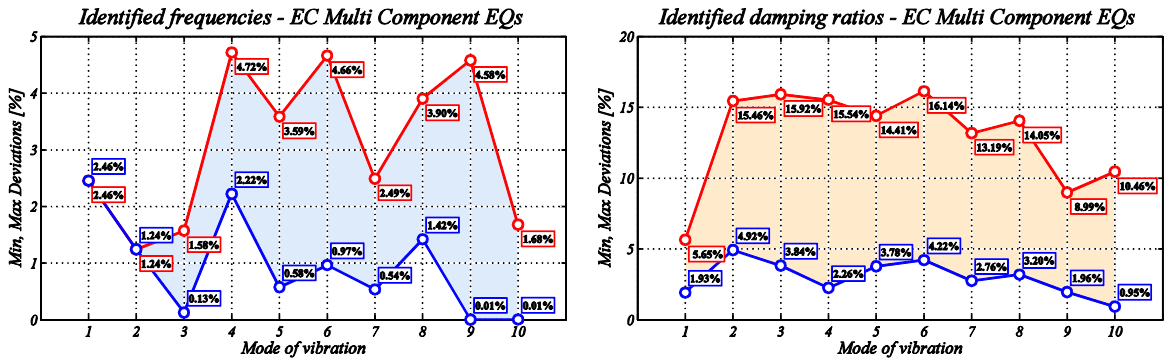

Figure 21: *Minimum and maximum deviations for identified frequencies and modal damping ratios (ranging from 2% to 9%), the ten-storey frame, El Centro earthquake: multi-component earthquakes.*

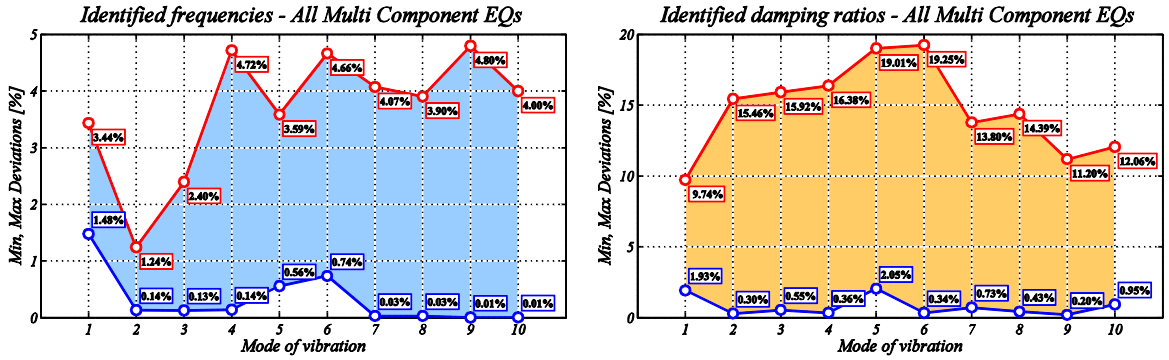

Figure 22: *Minimum and maximum deviations for identified frequencies and modal damping ratios (ranging from 2% to 9%), ten-storey frame, all adopted earthquakes: multi-component earthquakes.*

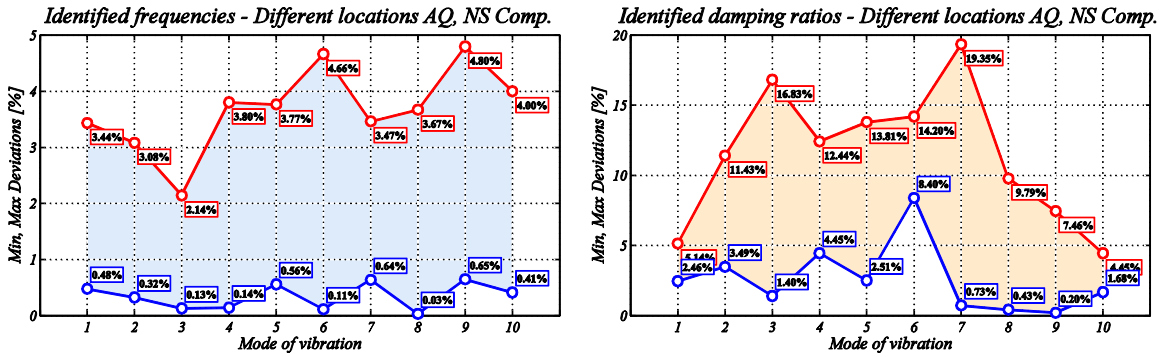

Figure 23: *Minimum and maximum deviations for identified frequencies and modal damping ratios (ranging from 2% to 9%), ten-storey frame, L'Aquila earthquake: NS component from different locations.*

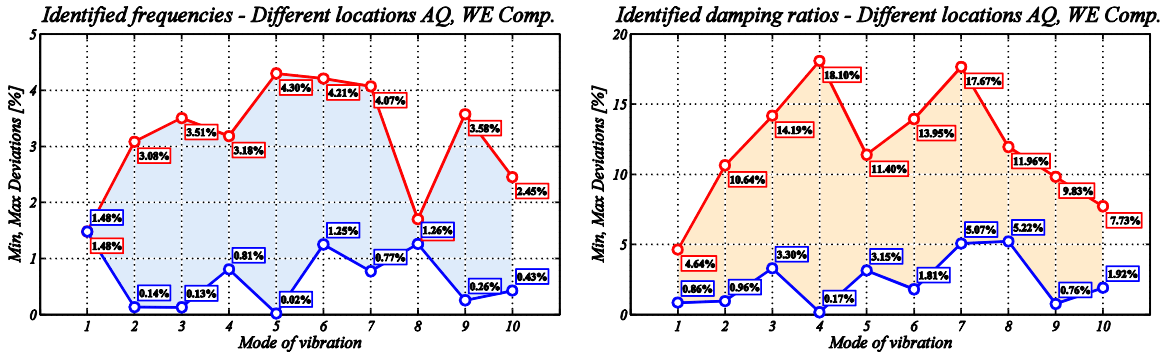

Figure 24: *Minimum and maximum deviations for identified frequencies and modal damping ratios (ranging from 2% to 9%) for the ten-storey frame, L'Aquila earthquake: WE component from different locations.*

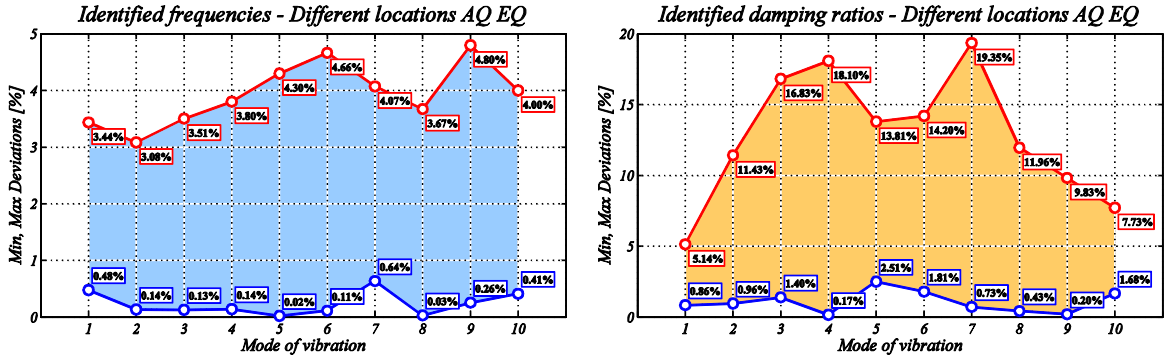

Figure 25: *Minimum and maximum deviations for identified frequencies and modal damping ratios (ranging from 2% to 9%) for the ten-storey frame, L'Aquila earthquake: NS and WE components from different locations.*

7. Conclusions

This paper has presented an independent implementation of a refined FDD algorithm towards reaching effective estimates of all structural modal parameters, i.e. natural frequencies, mode shapes and damping ratios at seismic input (and heavy damping). This method shall be able to identify the dynamic properties of civil structures from their recorded responses, with unknown input. Unlike the currently-available techniques in the Frequency Domain, especially classical FDD algorithms, which are strictly applicable only to stationary Gaussian white noise output data and weakly-damped structures, the proposed refined FDD algorithm is able to extract modal parameter estimates using earthquake response excitations, including for strong motion records and at concomitant heavy damping.

The algorithm has been assessed first on canonical force input based on random noise, acting on different ideal shear-type frame structures and from a realistic structure from the literature too. Then, modal identification is attempted successfully at seismic input, taken as ground excitation at the base of the same structures, both as SDOF and MDOF input. A set of three different strong ground motions with different characteristics, such as duration, frequency sampling, frequency content and power, has been employed. Also, attempts with multiple location earthquakes have been successfully performed. All cases exhibited very consistent results, in particular for the estimates of the natural frequencies, that are assessed with very high accuracy. Also, the other modal parameters are estimated with quite limited errors, and this holds true also for heavy-damped cases. The same is confirmed for the multi-component analyses and for the cases with added noise. Additionally to the present work, analyses with real earthquake response signals have been separately performed with the use of the rFDD algorithm, confirming the effectiveness of the method also in the real earthquake engineering range. The achieved results will be reported elsewhere [42].

Investigations and original arrangements about the processing of the PSD matrix, the use of untrended correlation functions, the importance of frequency resolution and of the prior filtering of data are thoroughly inspected, to reach reliable estimates of the modal parameters at seismic input. Further, careful treatments of spectral bell width, singular value and peak selection (with distinct or overlapped SVs too), and regression time window of the antitransformed signal have been located as crucial issues towards reaching valuable estimates, jointly with the use of the developed iterative loops.

Thus, the attempted simulations shall confirm the efficiency of the implemented algorithm, together with the possibility to perform FDD identification on earthquake response signals, also at concomitant heavy damping. It is shown that, in principle, FDD dynamic identification of structural modal properties of frames at seismic input shall be possible, with potential implications in the general realm of structural dynamics and, possibly, in the specific field of earthquake engineering, in view of characterizing the structural properties to be expected under seismic loading conditions.

Acknowledgements

The Authors would like to acknowledge public research funding from *"Fondi di Ricerca d'Ateneo ex 60%"* and a ministerial doctoral grant and funds at the ISA Doctoral School, University of Bergamo, Department of Engineering and Applied Sciences (Dalmine). The Authors would like to thank the anonymous reviewers involved in the review process for their valuable comments and suggestions, specifically for pointing out issues that have led to the extended analyses reported in Section 6.

References

[1] Maia M., Silva M. (Eds.), *Theoretical and Experimental Modal Analysis*, Taunton, England: Research Studies Press LTD, 1997.

[2] Karbhari V., Ansari F., *Structural Health Monitoring of Civil Infrastructure Systems*, Cambridge: Woodhead Publishing Limited, 2009.

[3] Garevski M., *Earthquakes and Health Monitoring of Civil Structures*, New York: Springer, 2013.

[4] Magalhães F., Cunha A., Caetano E., *Vibration based structural health monitoring of an arch bridge: from automated OMA to damage detection*, Mechanical Systems and Signal Processing, 28(4), pp. 212-228, 2012.

[5] Cara F.J., Juan J., Alarcon E., Reynders E., De Roeck G., *Modal contribution and state space order selection in operational modal analysis*, Mechanical Systems and Signal Processing, 38(2), pp. 276-298, 2013.

[6] Brincker R., *Ideas and Concepts of OMA - Lectures 1-6*, CISM Course 2010, 24-28 May 2010, Udine, Italy, 2010.

[7] Reynders E., *System identification methods for (Operational) Modal Analysis: review and comparison*, Archives of Computational Methods in Engineering, 19(1), pp. 51-124, 2012.

[8] Brincker R., Ventura C., Andersen P., *Why output-only modal analysis is a desiderable tool for a wide range of pratical applications*, Proceedings of the 21st International Modal Analysis Conference (IMAC-21), 3-6 February 2003, Kissimmee, Florida, pp. 265-272, 2003.

[9] Cunha A., Caetano E., *Experimental Modal Analysis of civil engineering structures*, Journal of Sound and Vibration, 40(6), pp. 12-20, 2006.

[10] Allemang R., Brown D., *A complete review of the complex mode indicator function (CMIF) with applications*, Proceedings of the International Conference on Noise and Vibration Engineering ISMA2006, Leuven, Belgium, 15-18 September 2006, pp. 3209-3246, 2006.

[11] Fladung W., Brown D., *Multiple reference impact testing*, Proceedings of SPIE - International Society for Optical Engineering, Los Angeles, California, 19-22 February 1993, pp. 1221-1229, 1993.

[12] Zhang L., Brincker R., Andersen P., *An overview of operational modal analysis: major developments and issues*, Proceedings of the 1st International Operational Modal Analysis Conference (IOMAC-05), 26-27 April 2005, Copenhagen, Denmark, pp. 171-177, 2005.

[13] Brincker R., Zhang L., *Frequency domain decomposition revisited*, Proceedings of 3rd International Operational Modal Analysis Conference, IOMAC'09, 4-6 May 2009, Portonovo (Ancona), Italy, pp. 615-626, 2009.

[14] Pioldi F., *Sulla stima dello smorzamento modale mediante algoritmo Frequency Domain Decomposition*, B.Sc. Thesis in Building Engineering, Advisor E. Rizzi, Università di Bergamo, Facoltà di Ingegneria, p. 169, 2012.

[15] Pioldi F., *Sulla formulazione di algoritmi ottimizzati di identificazione dinamica modale e loro applicazione in ambito sismico*, M.Sc. Thesis in Building Engineering, Advisor E. Rizzi, Università di Bergamo, Dipartimento di Ingegneria, p. 359, 2013.

[16] Brincker R., Zhang L., Andersen P., *Modal identification of output-only systems using frequency domain decomposition*, Smart Materials and Structures, 10(3), pp. 441-445, 2001.

[17] Gade S., Moller N., Herlufsen H., Konstantin-Hansen H., *Frequency domain techniques for Operational Modal Analysis*, Proceedings of the 21st International Modal Analysis Conference (IMAC-21), 3-6 February 2003, Kissimmee, Florida, pp. 17-26, 2003.

[18] Brincker R., Ventura C., Andersen P., *Damping estimation by frequency domain decomposition*, Proceedings of the 19th International Modal Analysis Conference (IMAC-19), 5-8 February 2001, Kissimmee, Florida, pp. 698-703, 2001.

[19] Zhang L., Tamura Y., *Damping estimation of engineering structures with ambient response measurements*, Proceedings of the 21st International Modal Analysis Conference (IMAC-21), 3-6 February 2003, Kissimmee, Florida, pp. 226-233, 2003.

[20] Brewick P., Smyth A., *An investigation of the effects of traffic induced local dynamics on global damping estimates using operational modal analysis*, Mechanical Systems and Signal Processing, 41(2), pp. 433-453, 2013.

[21] Zhang L., Wang T., Tamura Y., *A frequency-spatial domain decomposition (FSDD) technique for operational modal analysis*, Mechanical Systems and Signal Processing, 24(5), pp. 1227-1239, 2010.

[22] Wang T., Zhang L., Tamura Y., *An operational modal analysis method in frequency and spatial domain*, Earthquake Engineering and Engineering Vibration, 4(2), pp. 295-300, 2005.

[23] Ghahari S., Abazarsa F., Ghannad M., Taciroglu E., *Response-only modal identification of structures using strong motion data*, Earthquake Engineering and Structural Dynamics, 42(11), pp. 1221-1242, 2013.

[24] Doebling S., Farrar C., *The state of the art in structural identification of constructed facilities*, Report by ASCE - Committe on Structural Identification of Constructed Facilities, 1999.

[25] Beck J., Jennings P., *Structural identification using linear models and earthquake recordings*, Earthquake Engineering and Stuctural Dynamics, 8(2), pp. 145-160, 1980.

[26] Beck J., *System identification applied to strong motion records from structures*, Earthquake Ground Motion and its Effects on Structures, Datt S.K. (Ed.), ASME Publications, AMD-53, New York, pp. 109-134, 1982.

[27] Hart G., Yao J., *System identification in structural dynamics*, Journal of Engineering Mechanics ASCE, 103(6), pp. 1089-1104, 1977.

[28] Smyth A., Pei J., Masri S., *System identification of the Vincent Thomas Bridge using earthquakes records*, Earthquake Engineering and Structural Dynamics, 32(3), pp. 339-367, 2003.

[29] Pridham B., Wilson J., *Identification of base-excited structures using output-only parameter estimation*, Earthquake Engineering and Structural Dynamics, 33(1), pp. 133-155, 2004.

[30] Lin C., Hong L., Ueng Y., Wu K., Wang C., *Parametric identification of asymmetric buildings from earthquake response records*, Smart Materials and Structures,14(4), pp. 850-861, 2005.

[31] Ventura C.E., Brincker R., Andersen P., *Dynamic properties of the Painter Street Overpass at different levels of vibration*, Proceedings of the 6th International Conference on Structural Dynamics (EURODYN), Paris, France, 4-7 September 2005, pp. 167-172, 2005.

[32] Magalhães F., Cunha A., *Explaining operational modal analysis with data from an arch bridge*, Mechanical Systems and Signal Processing, 25(5), pp. 1431-1450, 2010.

[33] Bendat J., Piersol A., *Random Data, Analysis and Measurements Procedures*, New York: Wiley, 1986.

[34] Pioldi F., Ferrari R., Rizzi E., *A refined FDD algorithm for Operational Modal Analysis of buildings under earthquake loading*, Proceedings of 26th International on Noise and Vibration Engineering (ISMA2014), Leuven, Belgium, 15-17 September 2014, 15 pages, Paper ID 593, 2014.

[35] Welch P.D., *The use of Fast Fourier Transform for the estimation of Power Spectra: a method based on time averaging over short, modified periodograms*, IEEE Transactions on Audio and Electroacoustics, 15(2), pp. 70-73, 1967.

[36] Reynders E., Houbrechts J., De Roeck G., *Fully automated (operational) modal analysis*, Mechanical Systems and Signal Processing, 29(5), pp. 228-250, 2012.

[37] Allemang R., *The Modal Assurance Criterion - Twenty years of use and abuse*, Sound and Vibration Magazine, 37(8), pp. 14-23, 2003.

[38] Magalhães F., Cunha A., Caetano E., Brincker R., *Damping estimation using free decays and ambient vibration tests*, Mechanical Systems and Signal Processing, 24(5), pp. 1274-1290, 2010.

[39] Zanchi D., Zanoni D., *Identificazione dinamica modale di strutture mediante tecniche basate sul solo segnale di risposta*, M.Sc. Thesis in Building Engineering, Advisor E. Rizzi, Co-Advisor R. Ferrari, Università di Bergamo, Facoltà di Ingegneria, p. 255, 2011.

[40] Leurs W., Deblauwe F., Lembregts F., *Modal parameter estimation based on complex mode indicator function*, Proceedings of the 11th International Modal Analysis Conference (IMAC-11), Kissimmee, Florida, 1-4 February 1993, pp. 1035-1041, 1993.

[41] Villaverde R., Koyama L.A., *Damped resonant appendages to increase inherent damping in buildings*, Earthquake Engineering and Structural Dynamics, 22(6), pp. 491-507, 1993.

[42] Pioldi F., Ferrari R., Rizzi E., *Earthquake FDD modal identification of current building properties from real strong motion structural response signals*, Submitted for publication, 2014.

Appendix A. Main features of ideal shear-type frames

Mass and stiffness matrices are set fixed for every frame as reported below. Damping matrices have been assumed to be diagonal in modal coordinates and represented by different modal damping ratios in the numerical tests.

Two-storey frame:

- Mass matrix [kg]: $\mathbf{M} = 70000 \begin{bmatrix} 1 & 0 \\ 0 & 1 \end{bmatrix}$

- Stiffness matrix [N/m]: $\mathbf{K} = 10^8 \begin{bmatrix} 2.54 & -1.24 \\ -1.24 & 1.24 \end{bmatrix}$

Three-storey frame:

- Mass matrix [kg]: $\mathbf{M} = 144000 \begin{bmatrix} 1 & 0 & 0 \\ 0 & 1 & 0 \\ 0 & 0 & 1 \end{bmatrix}$

- Stiffness matrix [N/m]: $\mathbf{K} = \mathrm{u} \begin{bmatrix} 2 & -1 & 0 \\ -1 & 2 & -1 \\ 0 & -1 & 1 \end{bmatrix}$

$\mathrm{u} = 12\mathrm{E}(8\mathrm{J}_1 + \mathrm{J}_2)/\mathrm{h}^3$, $\mathrm{E} = 30 \cdot 10^9\ \mathrm{N/m^2}$, $\mathrm{J}_1 = 1.25 \cdot 10^{-3}\ \mathrm{m}^4$, $\mathrm{J}_2 = 5.2 \cdot 10^{-3}\ \mathrm{m}^4$, $\mathrm{h} = 3\mathrm{m}$.

Six-storey frame:

- Mass matrix [kg]:

$$\mathbf{M} = 144000\begin{bmatrix} 1 & 0 & 0 & 0 & 0 & 0 \\ 0 & 1 & 0 & 0 & 0 & 0 \\ 0 & 0 & 1 & 0 & 0 & 0 \\ 0 & 0 & 0 & 1 & 0 & 0 \\ 0 & 0 & 0 & 0 & 1 & 0 \\ 0 & 0 & 0 & 0 & 0 & 1 \end{bmatrix}$$

- Stiffness matrix [N/m]:

$$\mathbf{K} = \mathrm{u}\begin{bmatrix} 2.9 & -1.4 & 0 & 0 & 0 & 0 \\ -1.4 & 2.7 & -1.3 & 0 & 0 & 0 \\ 0 & -1.3 & 2.5 & -1.2 & 0 & 0 \\ 0 & 0 & -1.2 & 2.3 & -1.1 & 0 \\ 0 & 0 & 0 & -1.1 & 2.1 & -1 \\ 0 & 0 & 0 & 0 & -1 & 1 \end{bmatrix}$$

Appendix B. Main features of a real structure (from Villaverde and Koyama, 1993)

Floor mass and stiffness properties are set fixed as reported below, from bottom to top floor. Modal damping ratios are taken according to a classical Rayleigh's damping approach, i.e. by a linear combination of stiffness and mass matrices, as explained at the beginning of Section 6.

Floor	**Stiffness $\times 10^3$[kN/m]**	**Mass $\times 10^3$[kg]**
1	62.47	179
2	59.26	170
3	56.14	161
4	53.02	152
5	49.91	143
6	46.79	134
7	43.67	125
8	40.55	116
9	37.43	107
10	34.31	98

Table 7: *Properties of a real ten-storey frame (from Villaverde and Koyama, 1993).*